ผลของกระบวนการอบอ่อนต่อผิวฟิล์มที่ปลูกโดยแบบจำลองการปลูกชนิดโมเลกุลาร์บีมเอพิแทกซีด้วยกฎอาร์รีเนียส

นางสาวสมจินตนา พจน์พานิช

วิทยานิพนธ์นี้เป็นส่วนหนึ่งของการศึกษาตามหลักสูตรปริญญาวิทยาศาสตรมหาบัณฑิต
สาขาวิชาฟิสิกส์ ภาควิชาฟิสิกส์
คณะวิทยาศาสตร์ จุฬาลงกรณ์มหาวิทยาลัย
ปีการศึกษา 2555

ลิขสิทธิ์ของจุฬาลงกรณ์มหาวิทยาลัย

บทคัดย่อและแฟ้มข้อมูลฉบับเต็มของวิทยานิพนธ์ตั้งแต่ปีการศึกษา 2554 ที่ให้บริการในคลังปัญญาจุฬาฯ (CUIR)
เป็นแฟ้มข้อมูลของนิสิตเจ้าของวิทยานิพนธ์ที่ส่งผ่านทางบัณฑิตวิทยาลัย
The abstract and full text of theses from the academic year 2011 in Chulalongkorn University Intellectual Repository(CUIR)
are the thesis authors' files submitted through the Graduate School.

EFFECTS OF ANNEALING PROCESS ON FILM SURFACES GROWN BY MOLECULAR BEAM EPITAXY GROWTH MODEL WITH ARRHENIUS LAW

Miss Somjintana Potepanit

A Thesis Submitted in Partial Fulfillment of the Requirements
for the Degree of Master of Science Program in Physics
Department of Physics
Faculty of Science
Chulalongkorn University
Academic Year 2012
Copyright of Chulalongkorn University

Thesis Title	EFFECTS OF ANNEALING PROCESS ON FILM SURFACES GROWN BY MOLECULAR BEAM EPITAXY GROWTH MODEL WITH ARRHENIUS LAW
By	Miss Somjintana Potepanit
Field of Study	Physics
Thesis Advisor	Assistant Professor Patcha Chatraphorn, Ph.D.

Accepted by the Faculty of Science, Chulalongkorn University in Partial Fulfillment of the Requirements for the Master's Degree

....Dean of the Faculty of Science

(Professor Supot Hannongbua, Dr. rer. nat.)

THESIS COMMITTEE

....Chairman

(Associate Professor Mayuree Natenapit, Ph.D.)

....Thesis Advisor

(Assistant Professor Patcha Chatraphorn, Ph.D.)

....Examiner

(Assistant Professor Satreerat Hodak, Ph.D.)

....External Examiner

(Soontorn Chanyawadee, Ph.D.)

สมจินตนา พจน์พานิช : ผลของกระบวนการอบอ่อนต่อผิวฟิล์มที่ปลูกโดยแบบจำลองการปลูกชนิดโมเลกุลาร์บีมเอพิแทกซีด้วยกฎอาร์รีเนียส. (EFFECTS OF ANNEALING PROCESS ON FILM SURFACES GROWN BY MOLECULAR BEAM EPITAXY GROWTH MODEL WITH ARRHENIUS LAW) อ.ที่ปรึกษาวิทยานิพนธ์หลัก : ผศ.ดร. ปัจฉา ฉัตราภรณ์, 49 หน้า.

ปัจจุบันงานวิจัยส่วนใหญ่สนใจว่าจะลดความขรุขระของผิวฟิล์มอย่างไร กระบวนการอบอ่อนเป็นหนึ่งในเทคนิควิธีที่ให้ผลลัพธ์ที่ดีที่สุดในการลดความขรุขระของผิวที่ปลูกหลังจากกระบวนการตกสะสมของอะตอมสิ้นสุดลง เนื่องจากกระบวนการนี้ให้พลังงานความร้อนแก่อะตอมบนซับสเตรทเพื่อที่จะทำลายพันธะที่สร้างในระหว่างการตกสะสมและแพร่ไปยังตำแหน่งอื่นๆ แม้ว่าในการทดลองกระบวนการอบอ่อนนั้นจะถูกใช้อย่างแพร่หลาย กระบวนการนี้กลับไม่ถูกพิจารณาในการศึกษาการจำลองการปลูกส่วนใหญ่ วัตถุประสงค์ของงานนี้คือศึกษาบทบาทของกระบวนการอบอ่อนต่อผิวฟิล์มที่ปลูกโดยแบบจำลองการปลูกชนิดโมเลกุลาร์บีมเอพิแทกซีเมื่อกฎที่ควบคุมอัตราการแพร่ในการจำลองเป็นไปตามกฎอาร์รีเนียส ซึ่งผลที่ได้จากการจำลองนั้นตรงกับผลจากการทดลองที่ว่า พิล์มมีผิวเรียบยิ่งขึ้นด้วยกระบวนการอบอ่อน นอกจากนี้การศึกษาของสัณฐานวิทยาผิวฟิล์ม ความกว้างส่วนต่อประสาน และฟังก์ชันสหสัมพันธ์ พบว่า ความขรุขระของส่วนต่อประสานลดลงตามอุณหภูมิการอบอ่อนที่เพิ่มขึ้น เนื่องจากโอกาสของอะตอมที่จะแพร่ไปยังตำแหน่งที่มีจำนวนโคออร์ดิเนชันมากนั้นเพิ่มขึ้นอย่างมีนัยสำคัญกับอุณหภูมิ อย่างไรก็ตาม ที่อุณหภูมิสูงจะมีอัตราการหลุดของอะตอมสูงขึ้นและกระบวนการหลุดของอะตอมที่มักไม่ถูกพิจารณาในการจำลองต่างๆนั้นจะมีความสำคัญมากขึ้น ด้วยสาเหตุนี้เราจึงศึกษาผลของกระบวนการหลุดของอะตอมต่อผิวฟิล์มโดยการเปรียบเทียบสมบัติทางสถิติของฟิล์มที่ปลูกทั้งแบบมีและไม่มีการหลุดของอะตอม ผลปรากฏว่า เมื่ออุณหภูมิการอบอ่อนสูงขึ้นถึง 900 K สมบัติทางสถิติโดยรวมของฟิล์มนั้นจะไม่ถูกกระทบด้วยการหลุดของอะตอมอย่างมีนัยสำคัญ แต่จากสัณฐานวิทยาและสมบัติเฉพาะที่นั้นมีความแตกต่างกัน

ภาควิชา ฟิสิกส์ ลายมือชื่อนิสิต

สาขาวิชา ฟิสิกส์ ลายมือชื่อ อ.ที่ปรึกษาวิทยานิพนธ์หลัก

ปีการศึกษา 2555

5372348023 : MAJOR PHYSICS
KEYWORDS : ANNEALING / MOLECULAR BEAM EPITAXY MODEL / ARRHENIUS LAW

SOMJINTANA POTEPANIT : EFFECTS OF ANNEALING PROCESS ON FILM SURFACES GROWN BY MOLECULAR BEAM EPITAXY GROWTH MODEL WITH ARRHENIUS LAW. ADVISOR : ASST. PROF. PATCHA CHATRAPHORN, Ph.D., 49 pp.

Presently many researches focus on how to minimize roughness of a film surface. An annealing process is one of the most promising techniques which are used to reduce roughness of the grown surface after the deposition of an atom has ended because it provides thermal energy for atoms on the substrate to break bonds formed during its deposition and diffuse to other positions. Despite being commonly used experimentally, the annealing process is seldom included in growth simulation studies. The objective of this work is to study the role of annealing process on a film surface grown by Molecular Beam Epitaxy model when the law governing the diffusion rate in simulations follows the Arrhenius law. The simulation results agree with the experimental results that the film surface is smoother when the annealing process is applied. Moreover, studies of the film surface morphology, the interface width, and the correlation functions show that the roughness of the interface decreases as the annealing temperature is increased. This is because the chance for an atom to diffuse to positions with large coordination numbers increases significantly with temperature. However, at high temperature, the desorption rate of an atom is higher and the desorption process, which is usually neglected in simulations, can become significant. For this reason, we study the effect of desorption process on the film surface by comparing statistical properties of films grown with and without desorption of atoms. The results show that when the annealing temperature is above 900 K, global statistical properties of the film are not significantly affected by the desorption of atoms but the morphologies and local properties are distinguishable.

Department : Physics Student's Signature ....

Field of Study : Physics Advisor's Signature ....

Academic Year : 2012

ACKNOWLEDGEMENTS

I would like to express my gratitude to my advisor, Asst. Prof. Dr. Patcha Chatraphorn, for giving an opportunity to work in Semiconductor Physics Research Laboratory (SPRL). I would also like to thank her for her guidance throughout my study which I convert into driving forces for me to work hard and improve myself.

I would like to thank Assoc. Prof. Dr. Mayuree Natenapit, Asst. Prof. Dr. Satreerat Hodak and Dr. Soontorn Chanyawadee for taking the time from their busy schedules to be my dissertation committee. Their comments on this dissertation are very greatly appreciated.

I would also like to thank Asst. Prof. Dr. Kajornyod Yoodee, Asst. Prof. Dr. Sojiphong Chatraphorn, Asst. Prof. Dr. Surachate Limkumnerd and Dr. Chatchai Srinitiwarawong for many helpful suggestions to improve my work.

I especially thank Dr. Annop Wongwathanarat for his support. He always gives advice and assistance to me throughout my study.

I would like to thank everyone in SPRL for every comments and ideas which make my work more complete. Finally, I would like to thank all my family’s members who always encourage me to fulfill my goal.

This work was partially supported by Thailand Center of Excellence in Physics (ThEP) and the Special Task Force for Activating Research (STAR), Ratchadaphiseksomphot Endowment Fund, Chulalongkorn University through the Energy Materials Physics Research Group.

CONTENTS

	Page
ABSTRACT IN THAI	iv
ABSTRACT IN ENGLISH	v
ACKNOWLEDGEMENTS	vi
CONTENTS	vii
LIST OF TABLES	ix
LIST OF FIGURES	x
LIST OF ABBREVIATIONS	xiii
CHAPTER I INTRODUCTION	1
CHAPTER II NUMERICAL METHOD	4
2.1 Growth Process	4
2.1.1 Deposition Process	5
2.1.2 Diffusion Process	5
2.1.3 Desorption Process	8
2.2 Annealing Process	10
CHAPTER III QUANTITIES OF INTEREST	12
3.1 Morphology	12
3.2 Interface Width	12
3.3 Correlation Functions	15
CHAPTER IV RESULTS AND DISCUSSIONS	18
4.1 Annealing Process without Desorption on Films Grown by Molecular Beam Epitaxy Model with Arrhenius Law	18
4.2 Annealing Process with Desorption on Films Grown by Molecular Beam Epitaxy Model with Arrhenius Law	27
4.2.1 Effect of Annealing Temperatures	30
4.2.2 Effect of Desorption Energy	34

Page

CHAPTER V CONCLUSIONS 44

REFERENCES 46

VITAE 49

LIST OF TABLES

Table **Page**

2.1 Diffusion time of atoms with n nearest neighbors at various the substrate temperatures 6

2.2 Desorption time of atoms at different substrate temperatures 8

4.1 The roughness exponent values of $G-r$ plots in Fig. 4.5 calculated from power law fit to the data for $r \leq 8$ 26

4.2 Desorption time of atoms at various desorption energy when the substrate temperature is 850 K and 900 K 37

LIST OF FIGURES

Figure **Page**

2.1 Schematic depiction of MBE growth processes: deposition of atom A, diffusion of atom B, and desorption of atom C 4

2.2 The flow chart of MBE growth simulation steps 7

2.3 The flow chart of MBE growth with desorption 9

2.4 The flow chart of annealing process without desorption 10

2.5 The flow chart of annealing process with desorption 11

3.1 The interface width as a function of time 14

3.2 (a) The height–height correlation function $G(r)$ as a function of r from the MBE with Arrhenius law growth in the system $L \times L = 256 \times 256$ with $T_G = 750$ K at the time 10^4 s. (b) The correlation function for four values of q in the same system as (a). The plot shows the multifractality of film 17

4.1 A typical film surface morphology of MBE grown at $T_G = 750$ K without desorption for the time $t_G = 10^3$ s in the system 256×256. 19

4.2 A typical film surface morphology of the film grown as in Fig. 4.1 then annealed without desorption at $T_A = 720$ K for the time $t_A = 10^4$ s 21

4.3 Morphologies of the film grown as in Fig. 4.1 then annealed without desorption for time $t_A = 10^4$ s at (a) $T_A = 750$ K (b) $T_A = 800$ K (c) $T_A = 850$ K and (d) $T_A = 900$ K 22

4.4 The interface width $W(t)$ as a function of time for MBE grown at $T_G = 750$ K without desorption on a substrate 256×256 for the time $t_G = 10^3$ s then annealed with various temperatures T_A for the time $t_A = 10^4$ s 24

4.5 The standard height–height correlation functions $G(r)$ in (a) x and (b) y directions of the grown film on a substrate 256×256 without desorption at $T_G = 750$ K in the time $t_G = 10^3$ s then annealed for the time $t_A = 10^4$ s with different temperatures T_A 25

Figure **Page**

4.6 Height difference correlation functions of order $q=1-4$, from bottom to top in the main plots of the film grown by MBE without desorption with $T_G=750$ K at the time $t_G=10^3$ s. The solid lines are the power law fits to data for $r \le 8$ with slopes α'_q. Inset: closed–up plots 28

4.7 Height difference correlation functions $G_q(r)$, $q=1-4$, from bottom to top of the film grown in 4.6 then annealed without desorption for the time $t_A=10^4$ s at (a) $T_A=750$ K and (b) $T_A=900$ K. The solid lines are the power law fits to data for $r \le 8$ with slopes α'_q. The scales are fixed in all main plots while the insets show closed–up plots 29

4.8 A typical film surface morphology of MBE grown at $T_G=750$ K with $E_d=2.47$ eV for the time $t_G=10^3$ s in the system 256×256 31

4.9 A typical film surface morphology of the film grown as in Fig. 4.8 then annealed at $T_A=720$ K with $E_d=2.47$ eV for the time $t_A=10^4$ s 32

4.10 A typical film surface morphology of the film grown as in Fig. 4.8 then annealed with $E_d=2.47$ eV for the time $t_A=10^4$ s at (a) $T_A=750$ K (b) $T_A=800$ K (c) $T_A=850$ K and (d) $T_A=900$ K 33

4.11 The interface width W versus time t of the MBE grown with $T_G=750$ K on a substrate 256×256 at the time $t_G=10^3$ s then annealed for the time $t_A=10^4$ s in using different T_A with (opened symbols) and without (filled symbols) desorption 35

4.12 The height–height correlation function $G(r)$ as a function of separation r with (opened symbols) and without (filled symbols) desorption in the film grown at $T_G=750$ K then annealed at $T_A=900$ K for the time $t_A=10^4$ s 36

4.13 A typical morphology of MBE grown at $T_G=750$ K when the desorption energy is (a) $E_d=2.3$ eV and (b) $E_d=2.4$ eV at the time $t_G=10^3$ s in the system 256×256 39

4.14 A typical morphology of the film in Fig. 4.13 then annealed at $T_A=850$ K for the time $t_A=10^4$ s when the desorption energy is (a) $E_d=2.3$ eV and (b) $E_d=2.4$ eV 40

Figure **Page**

4.15 A typical morphology of the film in Fig. 4.13(b) then annealed at $T_A = 900$ K for the time $t_A = 10^4$ s when the desorption energy is $E_d = 2.4$ eV 41

4.16 The interface width $W(t)$ as a function of time in the MBE growth with $T_G = 750$ K at the time $t_G = 10^3$ s then annealed for the time $t_A = 10^4$ s with a) $T_A = 850$ K and b) $T_A = 900$ K when the desorption energy is varied 42

4.17 The height–height correlation function $G(r)$ as a function of separation r for MBE growth on a substrate 256×256 with $T_G = 750$K at the time $t_G = 10^3$ s then annealed for the time $t_A = 10^4$ s with $T_A = 900$ K when the desorption energy is $E_d = 2.4$ and 2.47 eV 43

LIST OF ABBREVIATIONS

Symbol	Definition	Page
L	substrate size	4
F	deposition rate	5
t_F	deposition time	5
t_G	growth time	5
t_R	diffusion time	5
n	number of nearest neighbors or bonds	5
v_0	characteristic frequency of atomic vibrations	5
k_B	Boltzmann constant	6
h	Planck constant	6
T	substrate temperature	6
τ	desorption time	8
E_d	desorption energy	8
t_A	annealing time	10
W	interface width	12
t	time	12
t_{sat}	saturation time or crossover time	13
β	growth exponent: $W \sim t^{\beta}$	13
α	roughness exponent: $W_{sat} \sim L^{\alpha}$	13
z	dynamical exponent: $t_{sat} \sim L^{z}$	13
G	height–height correlation function	15
r	distance between two lattice sites	15
α'	local roughness exponent: $G \sim r^{\alpha'}$	16
ξ	correlation length	16
G_q	generalized q^{th} correlation function	16
T_G	growth temperature	18
T_A	annealing temperature	18

CHAPTER I

INTRODUCTION

Nonequilibrium surface growth phenomena have been found in nature such as the progression of the edge of an ink droplet on a paper, the growth of bacteria colonies, and the interface of films. These create a wide interest in the study to characterize those surfaces. In thin film physics, there are three methods used to study the surface of a growing film (Barabasi and Stanley, 1995). The first method is experimental work that study structures and properties of the grown films and find growth process that leads to desirable films such as the atomic deposition techniques on crystal: Molecular Beam Epitaxy (MBE) technique. The second is theoretical study which uses continuum equations as a tool for understanding the behavior of various growth processes at large length scales. The third is simulation study that bridges theories and experiments by using many discrete atomistic growth models to understand the microscopic processes at the atomic level. These methods utilize scaling concepts in order to identify universality class of a growing surface from the scaling behavior of the interface. The universality class groups together film surfaces with the same asymptotic behavior, although the mechanisms of diffusion leading to the actual interface are different.

In recent years, the questions regarding how to control surface roughness and effects of the roughness have been extensively studied. This is because they are useful for applications in industries. Smooth surfaces are more suitable for some applications such as transistor biasing since a rough surface creates a poor contact causing unsatisfying electrical properties (Hong, 2008). For this reason, many research groups focus on minimizing roughness of a film surface. The experimental and computational results show that surface diffusion plays an important role in controlling roughness of a grown film surface (Neave et al., 1985; Tanaka, Suzuki, and Nishinaga, 1991; Xiao, Alexander and Rosenberger, 1991). In fact, a film surface is smoother when the diffusion rate of atoms on the surface is higher. On the other hand, the surface is rough

when the diffusion rate is small (Xiao and Ming, 1994). The main goal of this work is to study the role of a technique used to increase the diffusion of atoms on film surfaces called "annealing".

Many researches focus on effects of the annealing technique on many structures. For example, the amorphous carbon film annealed at temperatures up to 1000 ºC was found to transform into polycrystalline graphite (McCulloch and Merchant, 1996). Annealing process was also used to increase crystallinity in the nanofibre leading to larger Young's modulus in the system (Tan and Lim, 2006). In addition, behavior of Al–Cu thin film system was studied by using massive MD simulation (Kim et al., 2009). Their results show that the annealing process increases the diffusion of an atom on surfaces and reduces roughness of the interface. This is because this technique is a heat treatment which provides thermal energy for atoms on a surface to break the initial bonds formed during the deposition and diffuse to other positions after the deposition process has ended. In this dissertation, we study parameters which affect the annealing process on film surfaces grown by the MBE model. This is different from other researches because we fix the annealing time and increase the annealing temperature to be higher than the growth temperature instead. Roughness of the film surfaces are investigated via the study of the film surface morphology, the time evolution of the interface width, and the height–height correlation functions.

MBE growth studied here is one of the most important technological processes to produce high quality films with smooth flat surfaces (Arthur, 2002; Ohring, 2002). It is used for growing epitaxial film whose atomic arrangement of the film matches a crystallographic structure of the substrate (Palisaitis and Vasiliauskas, 2008). To understand microscopic processes at the atomic level in MBE technique, many atomistic and continuous models have been proposed (Das Sarma and Tamborenea, 1991; Barabasi and Stanley, 1995; Meng and Weinberg, 1996). From the detailed study of MBE, there are three relevant processes at the interface (Barabasi and Stanley, 1995; Pimpinelli and Villain, 1998): deposition of atoms or molecules on the interface, diffusion of deposited atoms on the surface, and desorption or evaporation of atoms from the interface. The diffusion rule considered here follows the Arrhenius law which is used in many works such as the study of MBE growth model under Ehrlich–Schwoebel potential barrier effects (Schinzer, Köhler and Reents, 2000; Chanyawadee, 2004) and Ballistic Deposition model on patterned substrates (Das Sarma et al., 1994; Chaiyasorn, 2007). Desorption process is seldom included in growth

simulation studies because the desorption rate is usually very small compared to the deposition and diffusion rates. However, when the substrate temperature is increased, such as during the annealing process, there is a possibility that desorption of surface atoms may not be negligible. For this reason, the desorption process is included in this work and effects of desorption on the film surface are investigated.

The structure of this dissertation is as follows. Descriptions of algorithms used in our simulations of these techniques for both the cases with and without desorption are presented in Chapter 2. Details of quantities used to analyze our numerical results are presented in Chapter 3. The computational results are shown in Chapter 4 where the role of annealing on films with various temperatures and the effect of desorption process on surfaces are discussed. Finally, we give a conclusion in Chapter 5.

CHAPTER II

NUMERICAL METHOD

Many atomistic models have been proposed for the study of thin film growth by Molecular Beam Epitaxy (MBE) (Das Sarma and Tamborenea, 1991; Barabasi and Stanley, 1995; Meng and Weinberg, 1996). This is because MBE is a technique used to produce a high quality film. Our work is to use an atomistic model to study the role of annealing on a film surface grown by MBE. The law governing the diffusion rate in our simulations follows the Arrhenius law. In this chapter, we describe algorithms used to simulate MBE growth and the annealing process.

2.1 Growth Process

MBE growth model studied here, which is performed in two dimensional substrate of the size $L \times L$, is restricted to obey solid–on–solid and periodic boundary conditions. In general, there are three relevant processes in MBE growth (Barabasi and Stanley, 1995; Pimpinelli and Villain, 1998): deposition, diffusion, and desorption process. These are shown in Fig. 2.1.

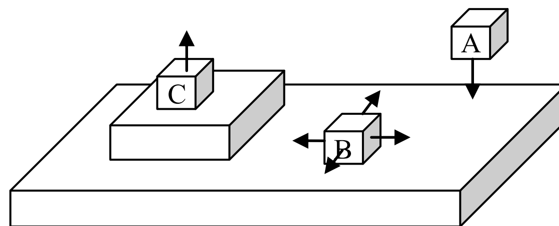

Figure 2.1: Schematic depiction of MBE growth processes: deposition of atom A, diffusion of atom B, and desorption of atom C.

2.1.1 Deposition Process

In experiments, an atom from the beam is randomly deposited on a substrate maintained at a fixed temperature in an ultra-high vacuum (UHV) environment (Arthur, 2002). To mimic the UHV condition, we consider that an atom is directly deposited on the substrate without colliding with other atoms from the beam and form bonds with its nearest neighbors at that position. The deposition rate F , defined as the number of layers of deposited atoms per unit time, is fixed at 1 ML/s in this work. This means $L \times L$ atoms are deposited on a substrate of the size $L \times L$ lattice sites during 1 second. The deposition time t_F is the time used by an atom during the deposition process. It is defined as

$$t_F = (F \times L \times L)^{-1}. \tag{2.1}$$

In our simulations, we fix the growth time at $t_G = 10^3$ s. Thus the total number of deposited atoms are $t_G \times L \times L$.

2.1.2 Diffusion Process

The diffusion time t_R is the time that an atom uses to diffuse to one of its nearest neighbor positions. It is calculated according to the Arrhenius Law (Barabasi and Stanley, 1995; Das Sarma and Tamborenea, 1991; Ghaisas and Das Sarma, 1992)

$$t_R = t_0 \exp\left[\frac{E_A}{k_B T}\right], \tag{2.2}$$

with the activation energy E_A usually taken to be $E_A = E_0 + nE_b$. E_0 is the activation energy of a free atom with no bond which is a result from the binding from other atoms on the substrate, e.g., atoms in the nearest neighbors. E_b is the bonding energy per bond and n is the number of nearest neighbor atoms or bonds. Normally, the preexponential constant is set to be $t_0 = v_0^{-1}$ where $v_0 = 2k_B T/h$ is the characteristic frequency of atomic vibrations in crystal (Kittel, 1971) when k_B

is the Boltzmann constant, h is the Planck constant and T is the substrate temperature. In our simulation, E_0 and E_b are chosen to be 1.0 eV and 0.3 eV, respectively, when the number of bonds is $n = 1, 2, ..., 5$ in order to be approximately consistent with Si and GaAs atoms (Das Sarma and Tamborenea, 1991, Barabasi and Stanley, 1995; Elsholz, Meixner and Schöll, 2003) which are prominent examples of films grown by MBE technique. From Eq. (2.2), it can be seen that the diffusion time is a function of number of bonds n and the substrate temperature T. The diffusion time increases with n because a larger amount of energy is required to break bonds that the atom formed during its deposition in order to diffuse to other positions. On the other hand, when T is increased, the diffusion time becomes smaller. This is because a high–temperature substrate can supply more energy to surface atoms so it is easier for them to break the previously formed bonds and diffuse. The values of t_R at various n and T are shown in Table 2.1.

In simulations, we choose a deposited atom with the smallest diffusion time on the surface to diffuse to one of its nearest neighbor sites. If there are many atoms with the same smallest t_R, one of them is chosen by random. Total time duration available for atoms on the substrate to diffuse before a new deposition is equal to the deposition time t_F. A flowchart describing algorithms in our simulations is shown in Fig. 2.2.

Table 2.1: Diffusion time of atoms with n nearest neighbors at various the substrate temperatures.

$t_{R(n)}$ (s)	720 K	750 K	800 K	850 K	900 K
$t_{R(n=1)}$	4.19×10^{-5}	1.74×10^{-5}	4.64×10^{-6}	1.44×10^{-6}	5.08×10^{-7}
$t_{R(n=2)}$	5.28×10^{-3}	1.80×10^{-3}	3.60×10^{-4}	8.66×10^{-5}	2.43×10^{-5}
$t_{R(n=3)}$	6.64×10^{-1}	1.87×10^{-1}	2.80×10^{-2}	5.20×10^{-3}	1.16×10^{-3}
$t_{R(n=4)}$	83.6	19.4	2.17	3.13×10^{-1}	5.56×10^{-2}
$t_{R(n=5)}$	1.05×10^{4}	2.02×10^{3}	1.68×10^{2}	18.8	2.66

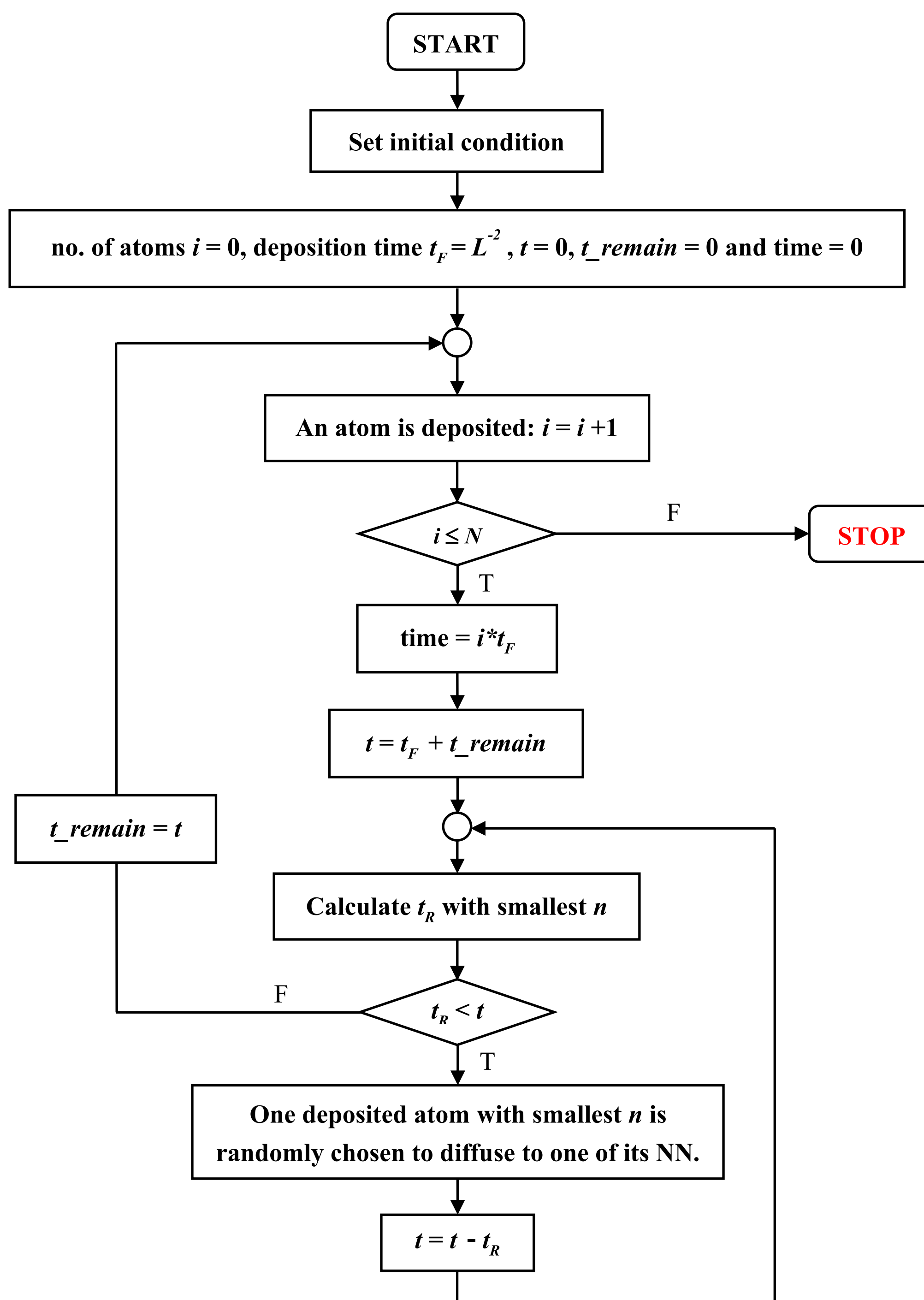

Figure 2.2: The flow chart of MBE growth simulation steps.

2.1.3 Desorption Process

Desorption is often neglected in most MBE growth simulations because its probability is much lower than deposition and diffusion. In order to study effects of the desorption process on films grown by MBE, we allow one atom with $n = 1$ to be removed from the surface during a time period of τ when τ is the desorption time. The desorption time is determined by (Barabasi and Stanley, 1995)

$$\tau = \tau_0 \exp\left[\frac{E_d}{k_B T}\right], \tag{2.3}$$

which is similar to the Arrhenius diffusion time in Eq. (2.2). τ_0 and E_d are the characteristic desorption time and energy, respectively. Their values are set to be $\tau_0 = 10^{-14}$ s and $E_d = 2.47$ eV (Barabasi and Stanley, 1995). Note that τ_0 has the same physical meaning as t_0 in Eq. (2.2) but its value is much smaller than the time t_0 at substrate temperature 900 K. The desorption time decreases when T is increased as shown in Table 2.2. This means that it is very difficult for an atom to desorb when the substrate temperature is low. A flowchart of the simulation steps for MBE growth with desorption is presented in Fig. 2.3.

Table 2.2: Desorption time of atoms at different substrate temperatures.

T (K)	**τ (s)**
750	396
800	36.3
850	4.42
900	0.678

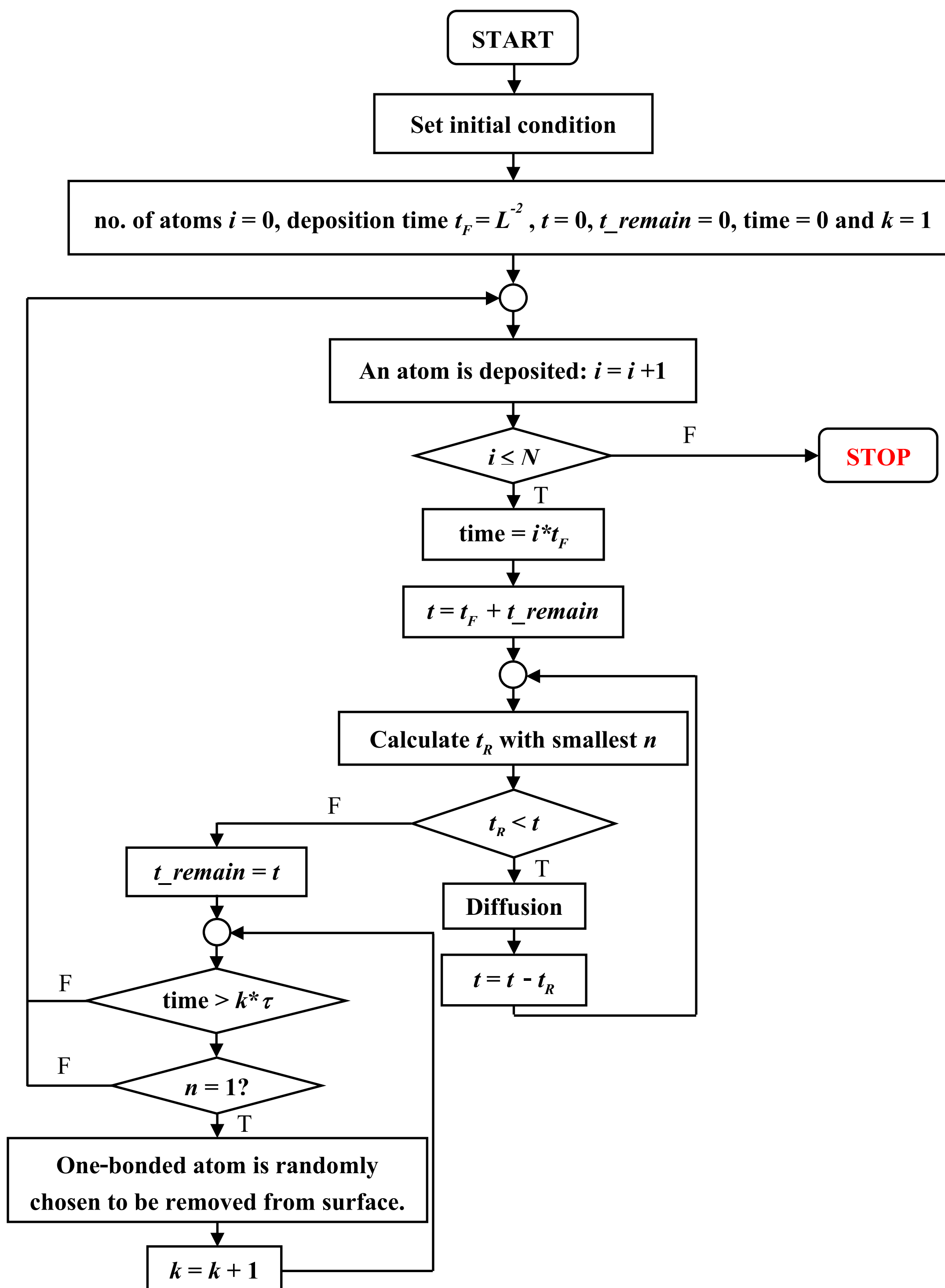

Figure 2.3: The flow chart of MBE growth with desorption.

2.2 Annealing Process

The growth process ends at a predetermined growth time t_G. After this, the as–grown film is obtained. The annealing process is then simulated at substrate temperature T_A. During the annealing process, atoms are allowed to diffuse without any deposition. An atom with the smallest bonds is randomly chosen to diffuse to one of its nearest neighbor sites until the provided annealing time t_A is reached. The simulation steps of annealing process without desorption is presented in Fig. 2.4. For the annealing process with desorption, both diffusion and desorption are allowed. The flow chart of annealing process with desorption is shown in Fig. 2.5.

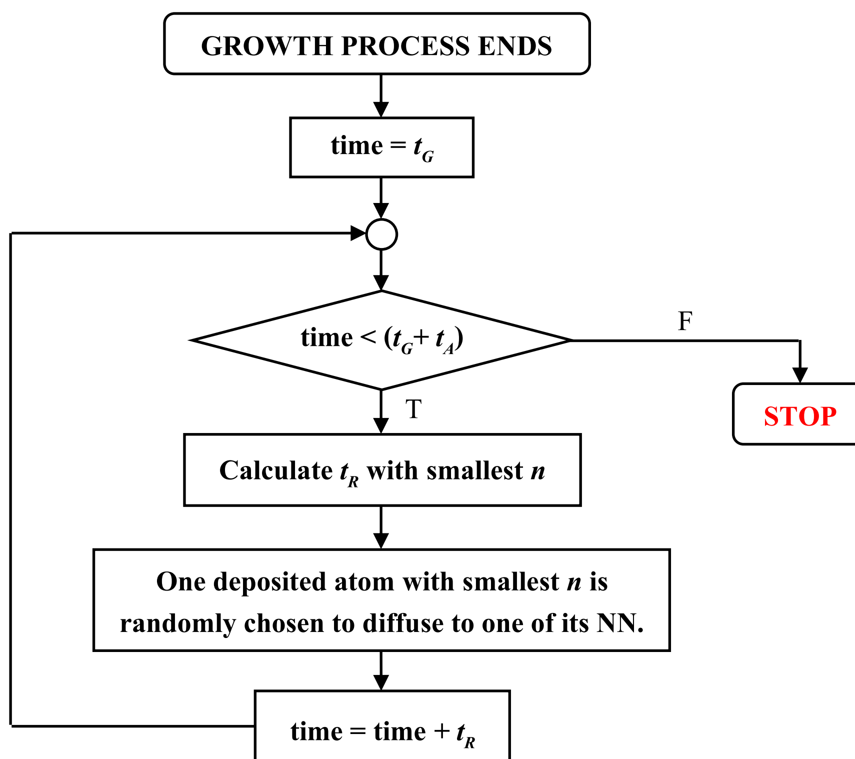

Figure 2.4: The flow chart of annealing process without desorption.

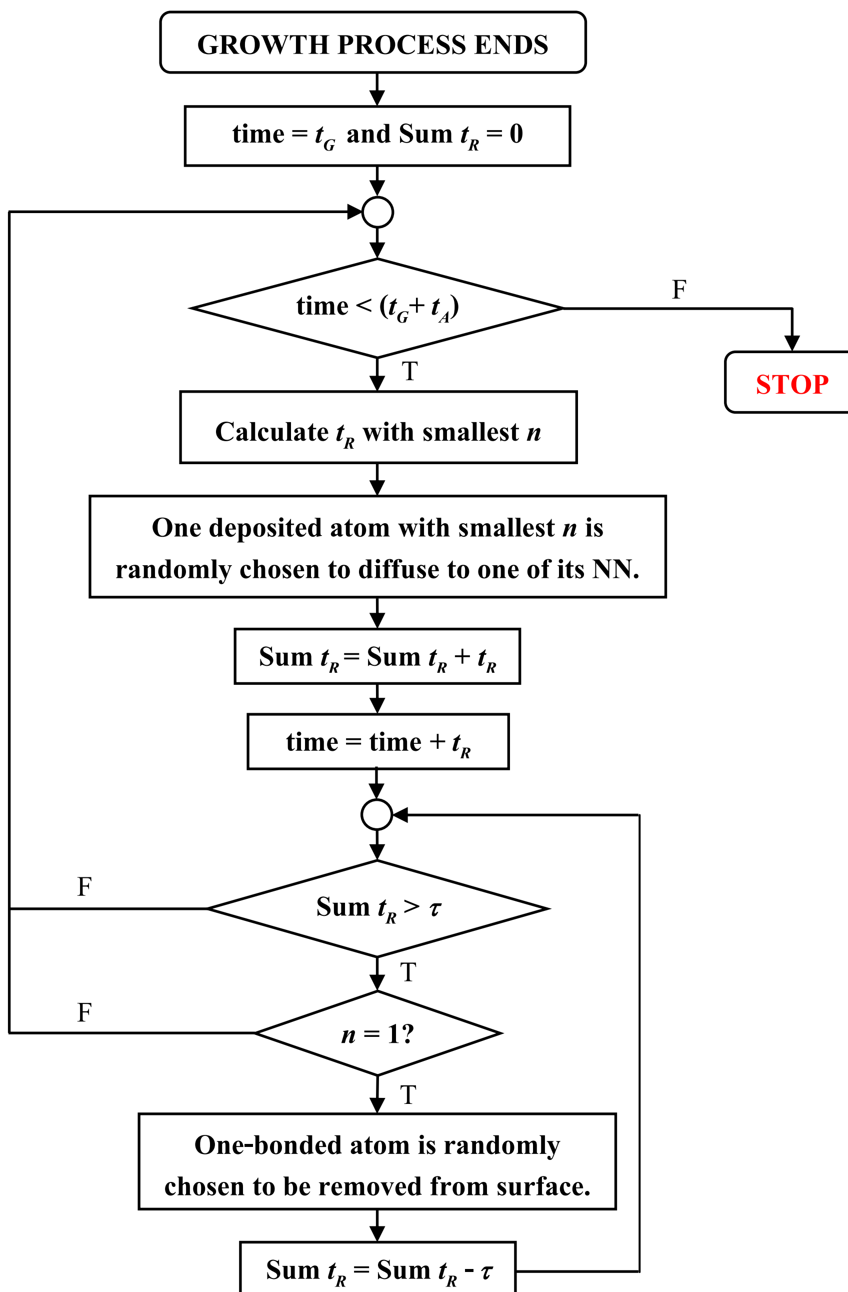

Figure 2.5: The flow chart of annealing process with desorption.

CHAPTER III

QUANTITIES OF INTEREST

Usually, roughness is used to study the quality of a grown film. We use it to identify the universality class of a thin film growth process. Roughness of a film surface can be studied by many statistical quantities. In this chapter, we introduce quantities that we use in order to characterize the roughness.

3.1 Morphology

Morphology of a film surface is the first thing that is usually observed. It shows the roughness on a film surface. In this thesis, morphologies are plotted in three dimensions. Both the x and y directions indicate the position $\vec{x}$ of an atom on a two dimensional substrate, while the z direction shows the height fluctuation of the film. The height $h(\vec{x})$ is defined as the number of occupied atoms at each position. The surface is flat $(h=0)$ at the initial time $(t=0)$.

3.2 Interface Width

Interface width, W, is one of the most important quantities used to characterize the roughness of a film surface. It is defined as the root mean square fluctuation of the height. Normally, the interface width is a function of the substrate size L and time t. In a system with a two–dimensional substrate, it is clearly defined (Barabási and Stanley, 1995; Punyindu, 2000; Aarão Reis, 2010) as

$$W(L,t) \equiv \sqrt{\frac{1}{L^2}\sum_{\vec{x}}[h(\vec{x},t)-\bar{h}(t)]^2}, \tag{3.1}$$

where $h(\bar{x},t)$ is the height at position $\bar{x}$ at time t and $\bar{h}(t)$ is the average height of the film at the same time t. In general, the time evolution of the interface width during kinetically rough growth mode has two regions separated by the saturation time or crossover time t_{sat}. In the early growth regime, the interface width increases as a power of time t. It scales as

$$W \sim t^{\beta} \qquad \text{when} \quad t \ll t_{sat}. \tag{3.2}$$

The exponent β is the *growth* exponent characterizing the time evolution of roughness. At later time, the interface width reaches a saturation value depending on the substrate size. It scales as

$$W_{sat} \sim L^{\alpha}, \qquad \text{when} \quad t \gg t_{sat}. \tag{3.3}$$

The exponent α is called the *roughness* exponent. It characterizes the roughness of a saturated interface. The saturation time is the time at which the growth behavior abruptly changes, as shown in Fig. 3.1. It depends on a substrate size as

$$t_{sat} \sim L^{z}, \tag{3.4}$$

where z is the *dynamical* exponent. At the saturation time, these exponents have a general relation as

$$z = \alpha / \beta. \tag{3.5}$$

These three exponents: β, α, and z are sometimes called the *critical* exponents. They are *global* exponents that describe global properties of the entire thin film. In numerical simulation, we usually use them to determine the universality class of the system which is a group of models with the same asymptotic behaviors.

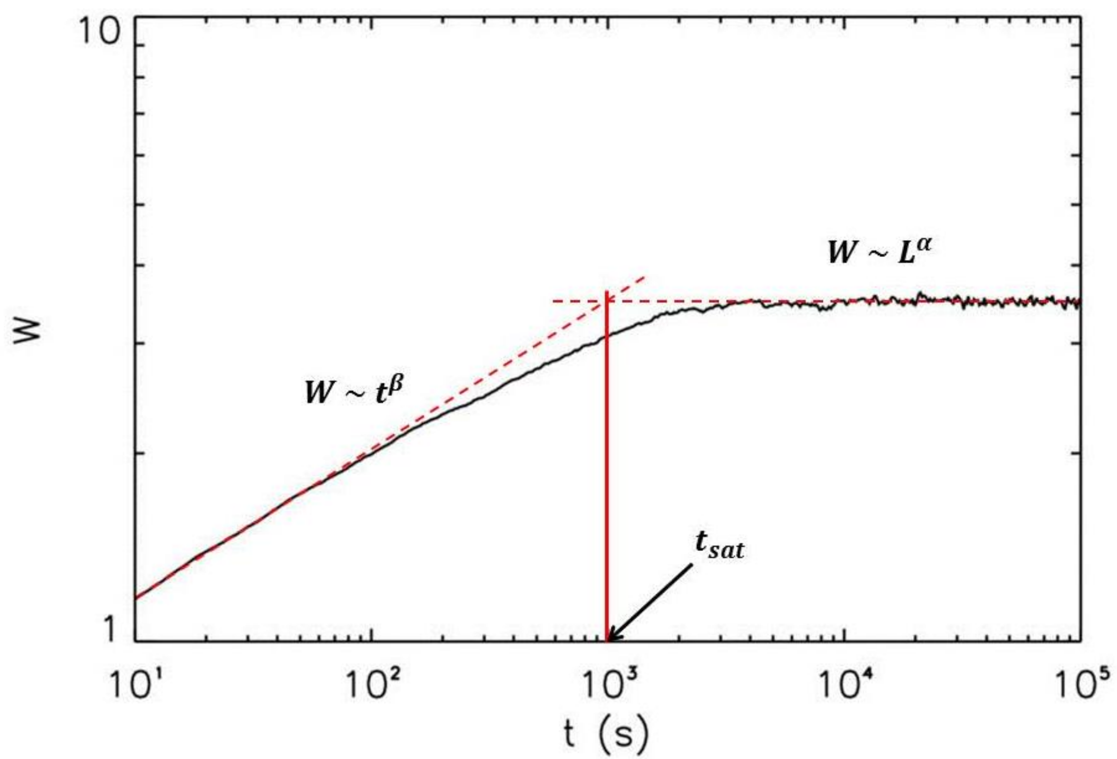

Figure 3.1: The interface width as a function of time (Changkaew, 2009).

3.3 Correlation Functions

Correlation functions, which are another interesting statistical quantity in thin film growths, are used to study the correlation of height between two lattice sites. For example, in the ballistic deposition (BD) model (Barabási and Stanley, 1995) the newly deposited atom sticks with the first nearest neighbor atom that it encounters. Therefore, the two lattice sites are correlated. The height of the site of the newly deposited atom, thus, is equal to or higher than the height of its neighbor site. In this work, we study effects of annealing process on the film surface grown by MBE model with Arrhenius law. This model also has correlations of the height between two lattice sites since its diffusion rule allows one of the atoms with the smallest bond diffuses to one of its nearest neighbors.

The correlation function studied here is the height–height correlation function $G(\bar{r},t)$. It is defined through the height difference at the same time. The height–height correlation functions describe the *local* behavior of films at time instant t. At a fixed time, the correlation function G is a function of the distance r and is defined for a two–dimensional film (Das Sarma, Ghaisas and Kim, 1994) as

$$G_x(r_x,t) \equiv \sqrt{\frac{1}{L^2}\sum_{x,y}\left[h(x+r_x,y,t)-h(x,y,t)\right]^2},$$

and

$$G_y(r_y,t) \equiv \sqrt{\frac{1}{L^2}\sum_{x,y}\left[h(x,y+r_y,t)-h(x,y,t)\right]^2}, \tag{3.6}$$

where $h(x,y,t)$ is the height at position (x,y) at time t and r_x and r_y are the distance between two lattice sites on the surface in the x– and y– direction, respectively. In this work, the system is isotropic and $G_x(r,t)=G_y(r,t)$ when $r_x = r_y = r$. Normally, the distance of interest is $r \le L/2$ for thin film grown with a periodic boundary condition. At small distances, the heights between any two sites are not independent and the correlation function G scales with the distance r as

$$G \sim r^{\alpha'}, \qquad \text{when} \quad r \ll \xi. \tag{3.7}$$

The exponent α' is called the *local roughness* exponent, and ξ is the *correlation length*. At large distances, the heights between any two sites are completely independent and the correlation function G becomes constant. The value of the saturated G depends on the growth time t as

$$G_{sat} \sim t^{\beta}, \qquad \text{when} \quad r \geq \xi . \tag{3.8}$$

The exponent β is the same growth exponent as in Eq. (3.2).

In the study of fractal behaviors, self-affine fractals are generally invariant under anisotropic transformations. If the growing surface is self-affine, the local roughness exponent α' is the same as the global roughness exponent α extracted from the time evolution of the interface width. For surfaces of some systems, however, the local and global exponents are different (Das Sarma, et al., 1996; Dasgupta, Das Sarma and Kim, 1996; López, 1999). This exhibits multi-affine behavior which has *q*–dependent exponents extracted from the correlation functions (Barabási, Szépfalusy and Vicsek, 1991; Barabási and Vicsek, 1991; Barabási et al., 1992). The detailed study of multifractality by Krug (Krug, 1994) defines the generalized height–height correlation function as

$$G_q(r,t) \equiv \left\langle \frac{1}{L^d} \sum_{x,y} \left| h(x+r, y, t) - h(x, y, t) \right|^q \right\rangle^{1/q} . \tag{3.9}$$

Note also that G of Eq. (3.6) can be found by substituting $q = 2$ into Eq. (3.9). Multi-affine scaling indicates *q*–dependent dynamical scaling properties of G_q as

$$G_q \sim r^{\alpha'_q}, \qquad \text{when} \quad r << \xi , \tag{3.10}$$

and

$$G_q \sim t^{\beta}, \qquad \text{when} \quad r \geq \xi . \tag{3.11}$$

Fig. 3.2 (a) shows the standard correlation function from the MBE model with Arrhenius law. The *q*–dependent roughness exponents α'_q illustrated by $G_q(r)$ plot in Fig. 3.2 (b) indicates strong multi-affine in its surface.

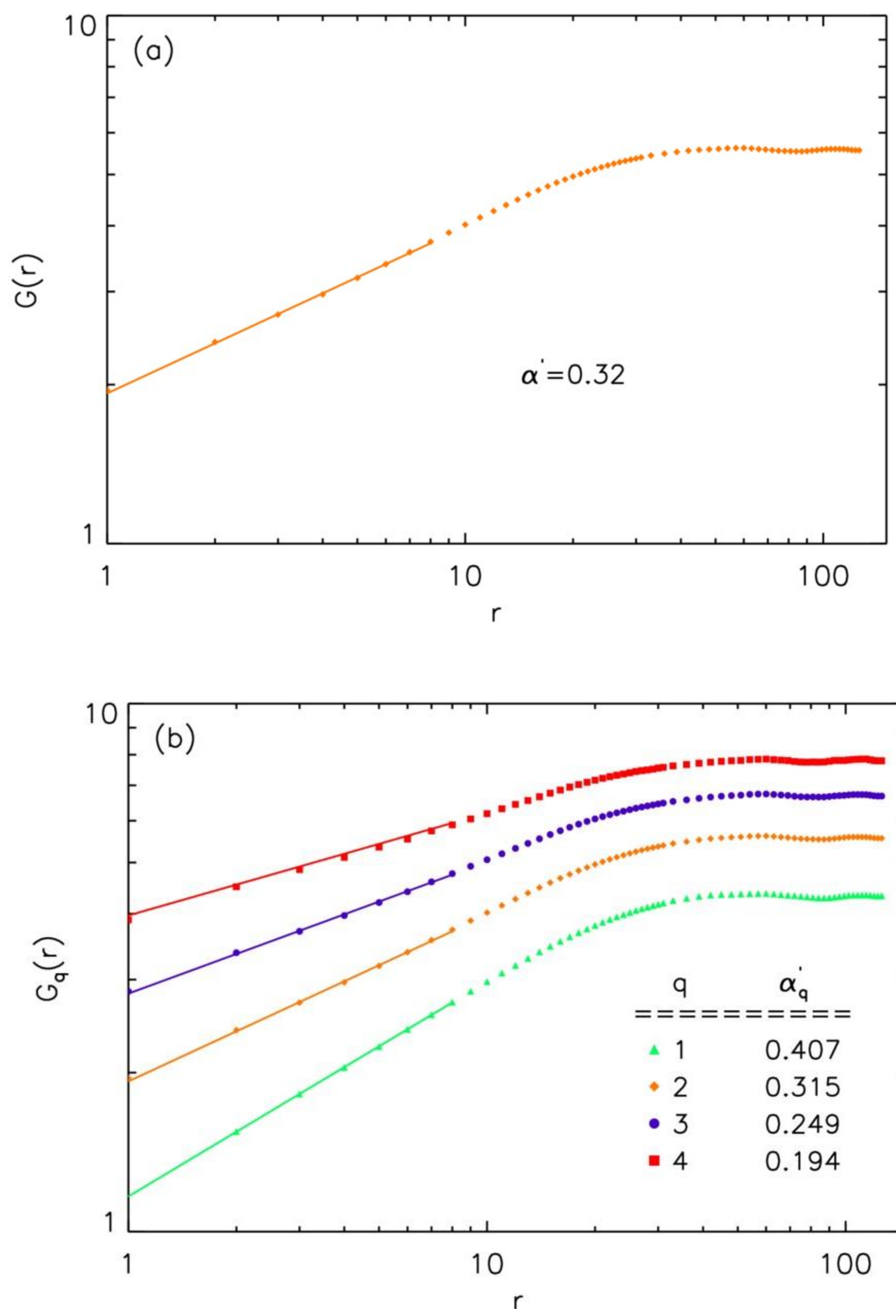

Figure 3.2: (a) The height–height correlation function $G(r)$ as a function of r from the MBE with Arrhenius law growth in the system $L \times L = 256 \times 256$ with $T_G = 750$ K at the time 10^4 s. (b) The correlation function for four values of q in the same system as (a). The plot shows the multifractality of film.

CHAPTER IV

RESULTS AND DISCUSSIONS

We have already explained the algorithms used to simulate thin films grown by MBE technique and annealed with the annealing temperature T_A. Details of statistical quantities used to study the grown films are discussed in chapter 3. In this chapter, effects of the annealing process on roughness of the interface are presented. Morphology, interface width, and correlation functions of films simulated under various growth conditions are discussed.

4.1 Annealing Process without Desorption on Films Grown by Molecular Beam Epitaxy Model with Arrhenius Law

In this section, we present effects of annealing process on the film surfaces when desorption of an atom is assumed to be negligible. To study how the annealing process affects roughness of the film surfaces, the annealing temperature T_A is varied within the range from 720 K to 900 K while the growth temperature T_G is fixed at $T_G = 750$ K. We grow the films by performing simulations on two−dimensional substrates of size 256×256 lattice sites with the deposition rate of 1 ML/s for the duration of $t_G = 10^3$ s. This means a total of 1000 MLs are deposited on the film surface at the end of the growth process. The surface of the grown film is shown in Fig. 4.1. It is very rough because the diffusion time of an atom with $n > 1$ at $T_G = 750$ K is larger than the deposition time so only atoms with $n = 1$ have a chance to diffuse. Nevertheless, the diffusing atoms on the surface cannot move far away from their deposited sites due to the fact that they are buried underneath by a newly deposited atom.

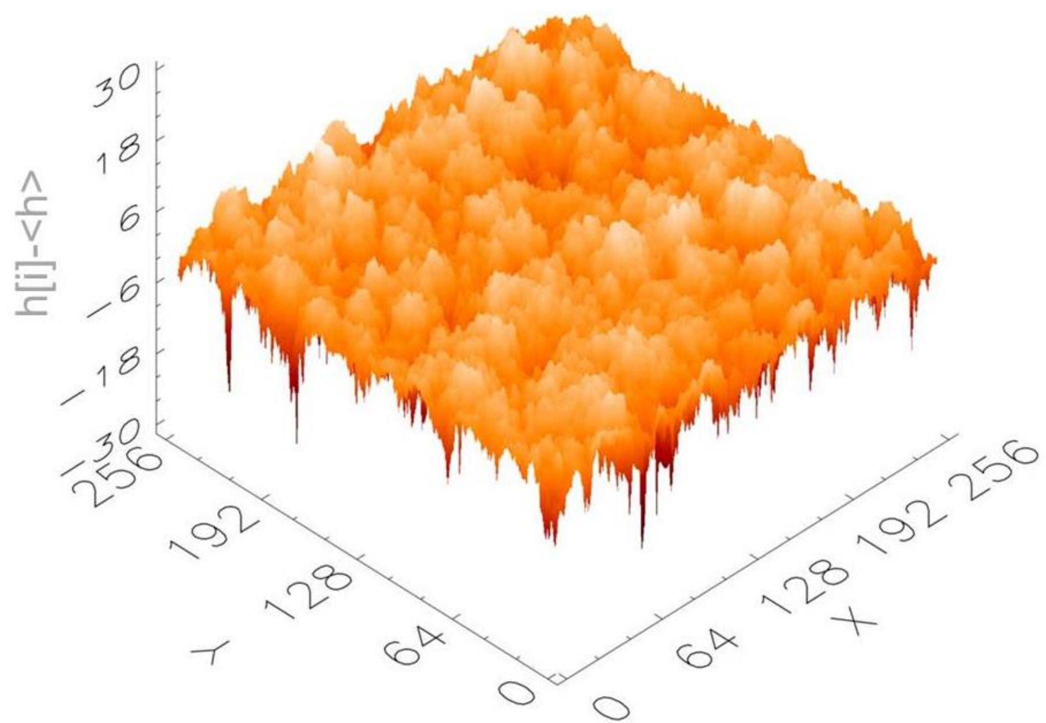

Figure 4.1: A typical film surface morphology of MBE grown at $T_G = 750$ K without desorption for the time $t_G = 10^3$ s in the system 256×256.

After the growth process ends at the predetermined time $t_G = 10^3$ s, the deposition is discontinued and the grown film is then annealed. Atoms on the surface are allowed to diffuse with the annealing temperature T_A until the annealing time $t_A = 10^4$ s is reached. A typical morphology of a film surface annealed with $T_A = 720$ K is shown in Fig. 4.2. It is not significantly different from the as–grown film (the completely grown film before the annealing process), although the surface atoms are allowed to diffuse without competing with the deposition during annealing process. This is because during diffusion in the annealing process, the chance of atoms with $n = 1$ or 2 to break bonds and diffuse is much higher than atoms with $n > 2$ as seen from their diffusion time in Table 2.1 (chapter 2). After these atoms diffuse, they form new bonds with the nearest neighbor atoms and the number of bonds becomes higher (n becomes larger than 2). Then the chance that these atoms continue to diffuse becomes much lower since the diffusion time of atoms with large n at $T_A = 720$ K, as displayed in Table 2.1, is very large. In general, the annealing temperature used in experiment is often lower than the growth temperature. However, the main interest is to minimize roughness of the as–grown film when the annealing time is fixed. Thus this study focusses on increasing the annealing temperature. The morphologies of films annealed at higher annealing temperatures: 750 K, 800 K, 850 K, and 900 K are shown in Fig. 4.3. The surfaces in Fig. 4.3 appear to be smoother than the one annealed at $T_A = 720$ K (Fig. 4.2) because the chance of an atom to diffuse to positions with large coordination numbers increases as T is increased. According to Eq. 2.2 in chapter 2, the diffusion time becomes significantly smaller when the temperature is higher. For example, the ratio of the diffusion time for an atom with $n = 1$ at the substrate temperature 900 K to the diffusion time at 750 K is approximately 0.03 as shown in Table 2.1 (chapter 2). This means that the number of times of atomic diffusion is much larger at 900 K than at 750 K. For this reason, the film of the system with the highest annealing temperature (Fig. 4.3 (d)) is the smoothest surface.

To proceed further, we use the statistical quantities such as the interface width and the correlation functions to analyze roughness of the interface. In this work, we perform the simulations using 5 different initial seeds for the random number generator and calculate the statistical quantities by using the ensemble averages. The time evolution of the root–mean–square height fluctuation (interface width) W in the systems without desorption process grown with

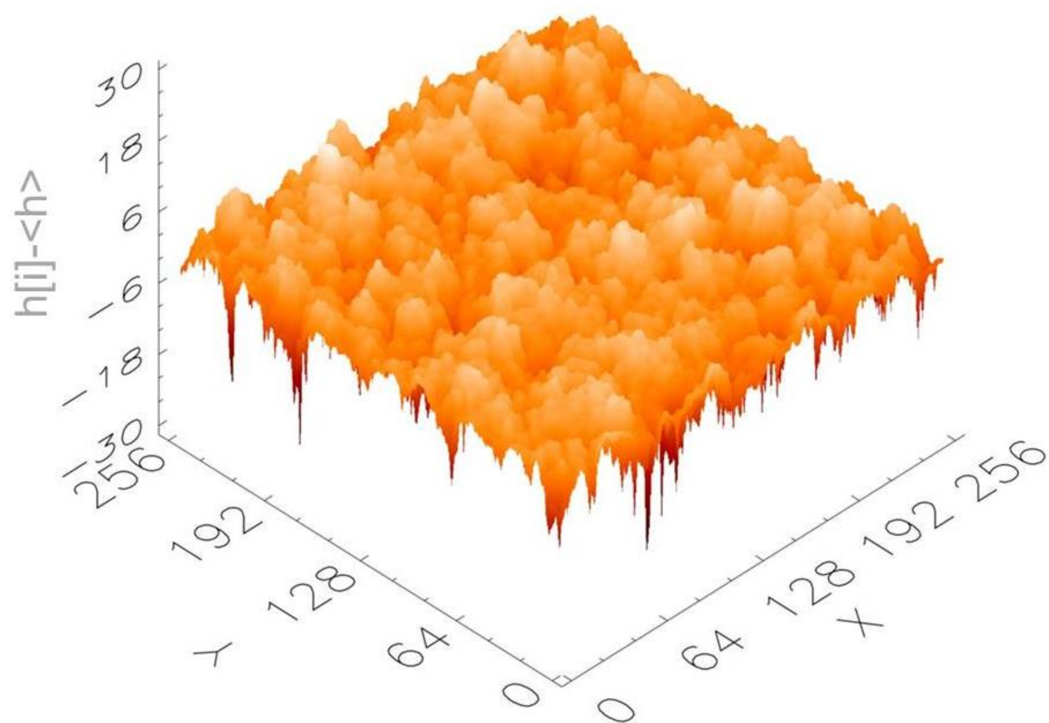

Figure 4.2: A typical film surface morphology of the film grown as in Fig. 4.1 then annealed without desorption at $T_A = 720\,\mathrm{K}$ for the time $t_A = 10^4$ s.

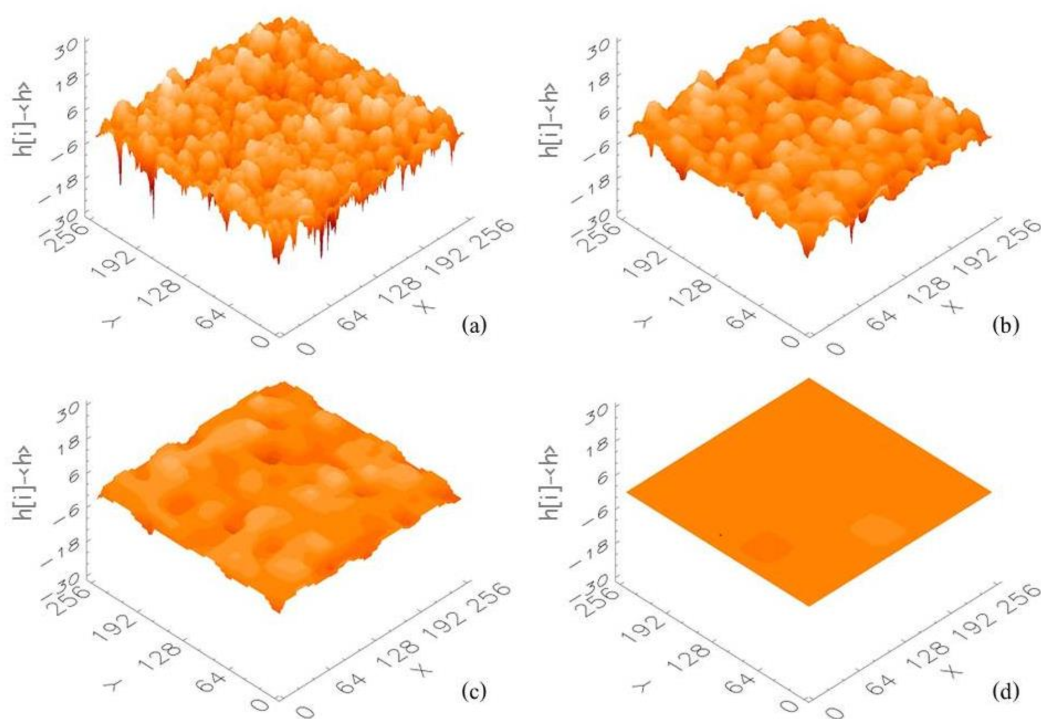

Figure 4.3: Morphologies of the film grown as in Fig. 4.1 then annealed without desorption for time $t_A = 10^4$ s at (a) $T_A = 750$ K (b) $T_A = 800$ K (c) $T_A = 850$ K and (d) $T_A = 900$ K.

with $T_G = 750\,\text{K}$ at $t_G = 10^3\,\text{s}$ and then annealed for the time $t_A = 10^4\,\text{s}$ with various annealing temperatures T_A are shown in Fig. 4.4. During the film growth process $(t < t_G)$, the W curve rises continuously with time. However, when the growth process has completed and the annealing process has started $(t > t_G)$, the interface width begins to decrease. This exhibits the strong effect of the annealing process in minimizing roughness of the interface. Furthermore, the higher annealing temperature helps decreasing roughness of the film surface. This can be inferred from the decline of the W curve shown in Fig. 4.4. The value of W from the film annealed with the highest annealing temperature (square symbols) is the smallest. It implies that the surface of film annealed at $T_A = 900\,\text{K}$ is the smoothest which is consistent with its film surface morphologies shown in Fig. 4.3(d).

A log – log plot of the standard height–height correlation functions G as a function of the separation distance r is presented in Fig. 4.5. It shows the correlation functions in both the x and y directions. We study the system in term of the local roughness exponents α' defined by $G \sim r^{\alpha'}$ when $r << \xi$. Note that the parameters α' do not indicate the roughness of the interface because their values are not used to identify the universality class of the system with anomalous and multiaffine scaling (Das Sarma, et al., 1996). The values of the exponent α' in both directions are listed in Table 4.1. The exponents obtained from $G - r$ plot in both directions are approximately equal which means that the system is isotropic. The film is statistically indifferent along the x and y directions because the chance of an atom to diffuse is equal in both directions. Numerical values of the height–height correlation function, $G(r) \sim \left\langle \sqrt{|h(x+r) - h(x)|^2} \right\rangle$, of the grown film with $T_G = 750\,\text{K}$ at $t_G = 10^3\,\text{s}$ displayed in Fig. 4.5 decreases when the film is annealed with different T_A for the time duration $t_A = 10^4\,\text{s}$. This indicates that the roughness of the interface is reduced by the annealing process because a small G value means that the height difference between two lattice sites is small. In the plots, the value of G decreases when T is increased and the film with the highest annealing temperature (square symbols) yields the smallest G value, which implies that its surface is the smoothest. This is in agreement with results inferred from the morphologies and the interface width.

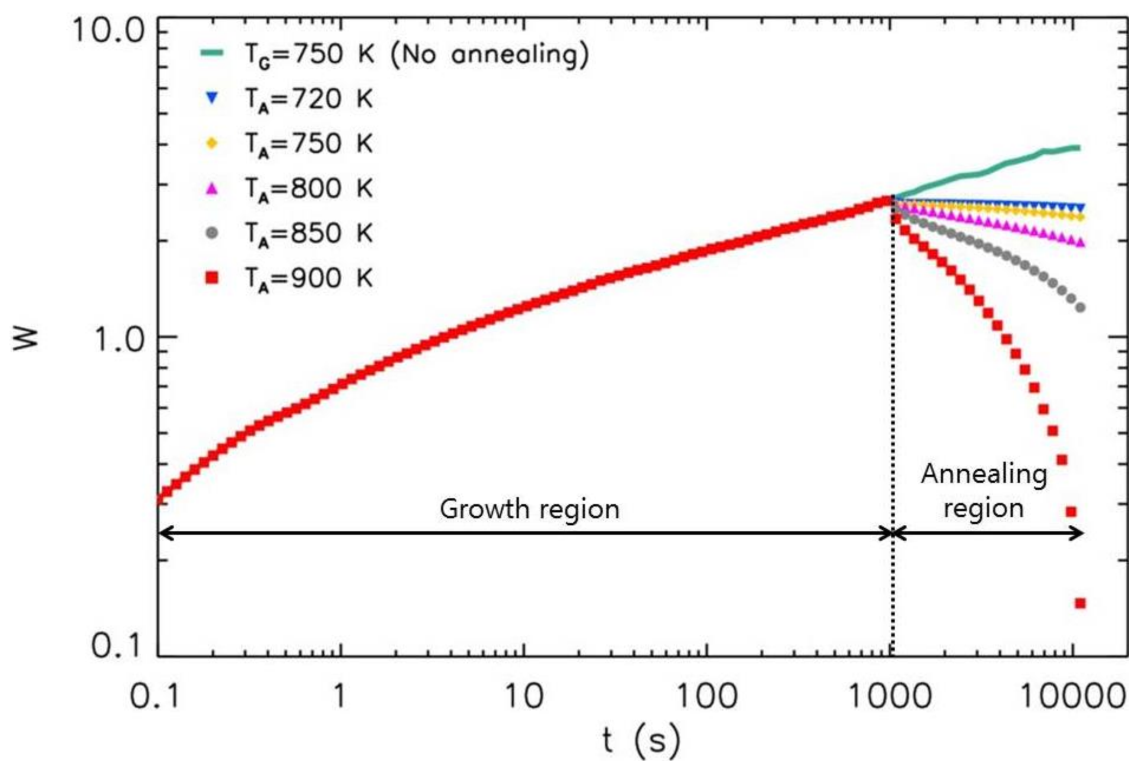

Figure 4.4: The interface width $W(t)$ as a function of time for MBE grown at $T_G = 750$K without desorption on a substrate 256×256 for the time $t_G = 10^3$ s then annealed with various temperatures T_A for the time $t_A = 10^4$ s.

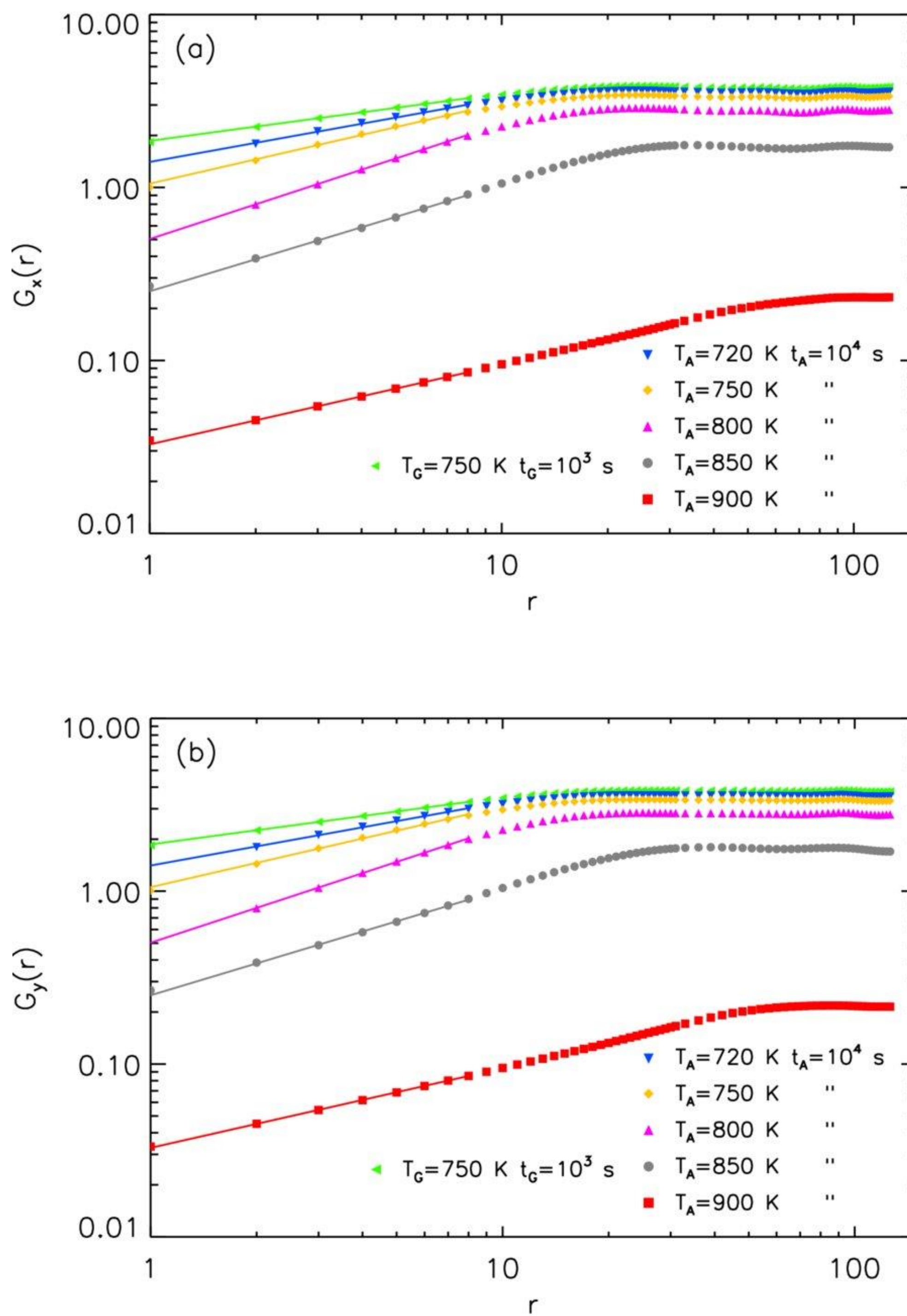

Figure 4.5: The standard height–height correlation functions $G(r)$ in (a) x and (b) y directions of the grown film on a substrate 256×256 without desorption at $T_G = 750$ K in the time $t_G = 10^3$ s then annealed for the time $t_A = 10^4$ s with different temperatures T_A.

Table 4.1: The roughness exponent values of $G-r$ plots in Fig. 4.5 calculated from power law fit to the data for $r \leq 8$.

	Films grown with $T_G = 750$ K	**Films annealed with various T_A**				
		720 K	**750 K**	**800 K**	**850 K**	**900 K**
α'_x	0.273	0.367	0.467	0.666	0.615	0.461
α'_y	0.273	0.368	0.468	0.669	0.613	0.461

To characterize fractal properties of the growing surface, we show the qth order height difference correlation functions G_q of the film grown with $T_G = 750$ K at $t_G = 10^3$ s in Fig. 4.6. The strong multifractality of the grown film is clearly seen from the differences between curves presented in Fig. 4.6. This demonstrates that these G_q functions have q–dependent local roughness exponent values. The local roughness exponent values are obtained from a power law fit to the data for $r \le 8$. From the plot, $\alpha'_1 = 0.354$, $\alpha'_2 = 0.273$, $\alpha'_3 = 0.218$, and $\alpha'_4 = 0.175$. In addition, the multiscaling behavior of the film annealed with $T_A = 750$ K and $T_A = 900$ K for the time $t_A = 10^4$ s is presented in Fig. 4.7. Note that Figs. 4.6 and 4.7 are plotted using the same scale for easy comparison. The values of G_q of the as–grown film (Fig. 4.6) and the film annealed at $T_A = 750$ K (Fig. 4.7(a)) are much larger than that of the film annealed at $T_A = 900$ K (Fig. 4.7(b)). This indicates that the film annealed at $T_A = 900$ K is much smoother. The results here agree with the morphologies shown earlier. However, as can be seen from the $G_q - r$ plots of the annealed films in Fig. 4.7, the α'_q exponents still have q–dependent indicating that the annealed films still exhibit multi-affine behavior in the same way as the as–grown films. We obtain $\alpha'_1 = 0.659$, $\alpha'_2 = 0.467$, $\alpha'_3 = 0.353$, and $\alpha'_4 = 0.262$ from the best fit to the same data in the film annealed with $T_A = 750$ K shown in Fig. 4.7(a). For the film annealed with $T_A = 900$ K, the α'_q values obtained from the data shown in Fig. 4.7(b) are $\alpha'_1 = 0.994$, $\alpha'_2 = 0.461$, $\alpha'_3 = 0.273$, and $\alpha'_4 = 0.184$. This demonstrates that the annealed films still have strong multifractality, although its morphology is very smooth.

4.2 Annealing Process with Desorption on Films Grown by Molecular Beam Epitaxy Model with Arrhenius Law

In thin film growth simulations, the desorption process is usually neglected because the desorption rate is much smaller than the deposition and diffusion rate. Nevertheless, the desorption rate becomes higher and more important when the substrate temperature increases.

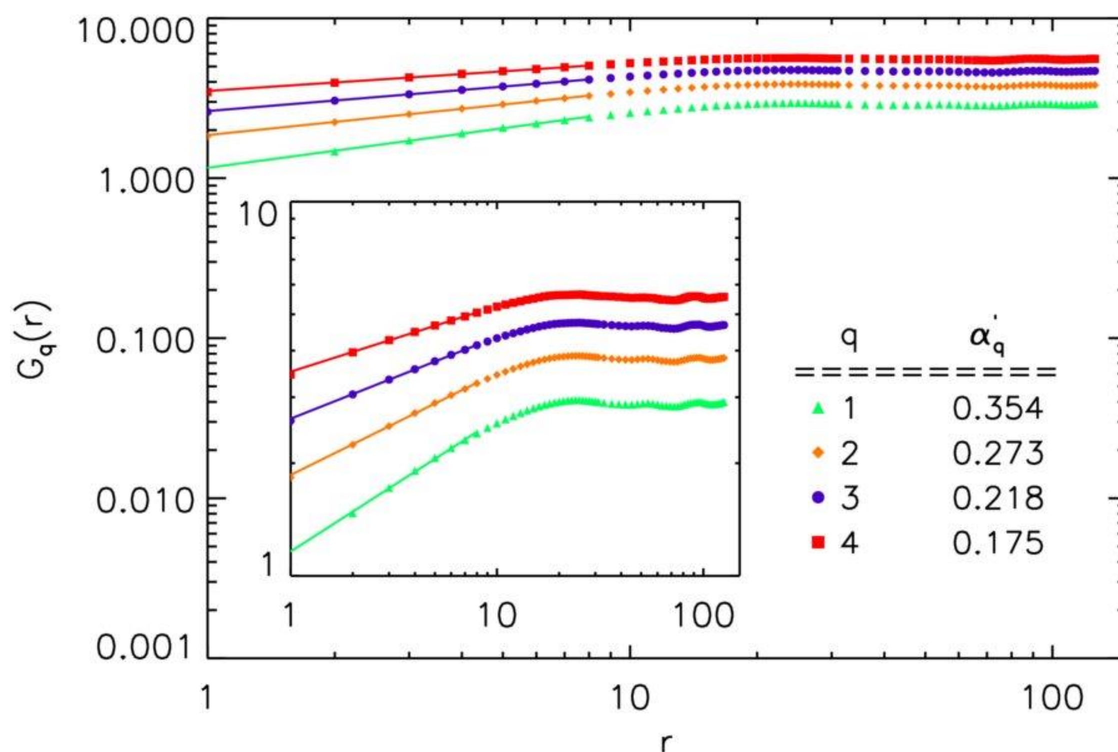

Figure 4.6: Height difference correlation functions of order $q = 1 - 4$, from bottom to top in the main plots of the film grown by MBE without desorption with $T_G = 750$ K at the time $t_G = 10^3$ s. The solid lines are the power law fits to data for $r \leq 8$ with slopes α'_q. Inset: closed–up plots.

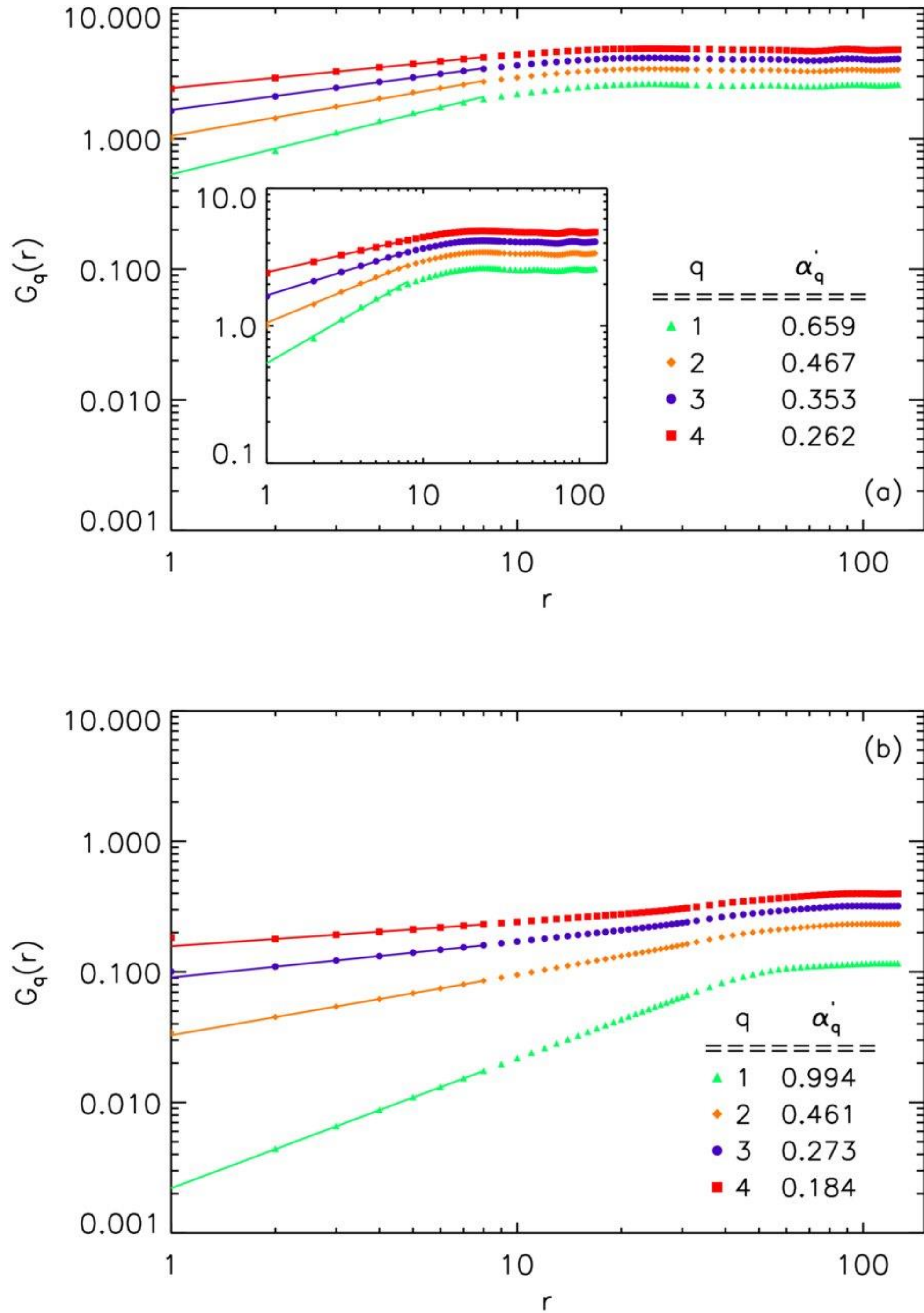

Figure 4.7: Height difference correlation functions $G_q(r)$, $q = 1-4$, from bottom to top of the film grown in 4.6 then annealed without desorption for the time $t_A = 10^4\,\mathrm{s}$ at (a) $T_A = 750\,\mathrm{K}$ and (b) $T_A = 900\,\mathrm{K}$. The solid lines are the power law fits to data for $r \le 8$ with slopes α'_q. The scales are fixed in all main plots while the insets show closed–up plots.

For this reason, the question "what is the difference between films grown with and without desorption?" arises. Therefore, we investigate the issue by including the desorption process into our simulations and compare the resulting film surfaces to the ones without desorption using the analysis of the film surface morphology, the interface width, and the correlation functions as explained in the previous chapter.

4.2.1 Effect of Annealing Temperatures

According to Eq. (2.3) presented in chapter 2, the desorption time is calculated from $\tau = \tau_0 \exp\left[E_d / kT\right]$ (Barabasi and Stanley, 1995) where T is the substrate temperature and E_d is the characteristic desorption energy of an atom. To study the difference of annealing process with and without desorption process on a film surface, the desorption energy of an atom is fixed at $E_d = 2.47$ eV (Barabasi and Stanley, 1995) while the film is grown and annealed at the temperature as specified in the previous section. A typical surface of a film grown by MBE with desorption at $T_G = 750$ K for the time $t_G = 10^3$ s on a system of the substrate size 256×256 lattice sites is shown in Fig. 4.8. The film surface appears to be very rough, and it is indistinguishable from the one without desorption (Fig. 4.1). This is because the desorption time at $T_G = 750$ K is very large. As a result, only a few atoms are desorbed from the interface within the considered growth time.

In Figs. 4.9 and 4.10, we show typical surfaces of films annealed with different annealing temperatures T_A within the range from 720 K to 900 K for the time $t_A = 10^4$ s when the desorption energy ($E_d = 2.47$ eV) is applied. The results of annealing with desorption can be seen in their morphologies. It appears that the morphologies of film surfaces do not differ significantly from the morphologies of films annealed without desorption, except for the films annealed at the highest annealing temperature $T_A = 900$ K. The morphologies of the film surfaces with and without desorption at $T_A = 900$ K become distinguishable. It is clearly seen that the surface of film with desorption at $T_A = 900$ K (Fig. 4.10(d)) is eroded and not as smooth as the one shown in Fig. 4.3(d). This is because the desorption process take away some of the atoms on the surface causing deterioration in the film surface.

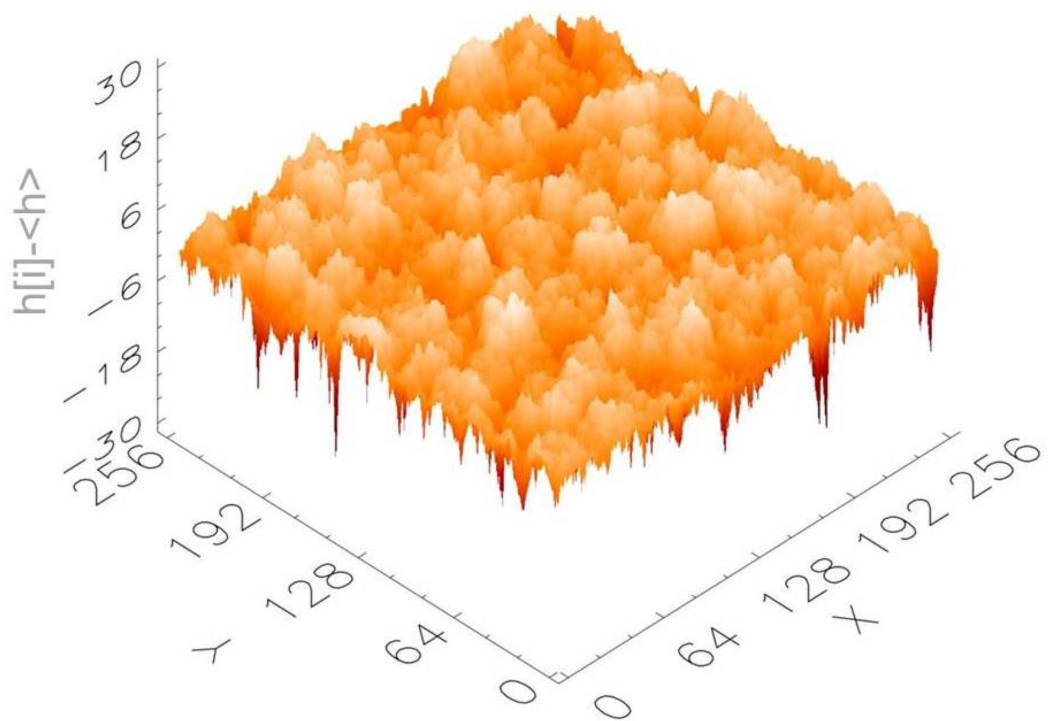

Figure 4.8: A typical film surface morphology of MBE grown at $T_G = 750\,\mathrm{K}$ with $E_d = 2.47\,\mathrm{eV}$ for the time $t_G = 10^3\,\mathrm{s}$ in the system 256×256.

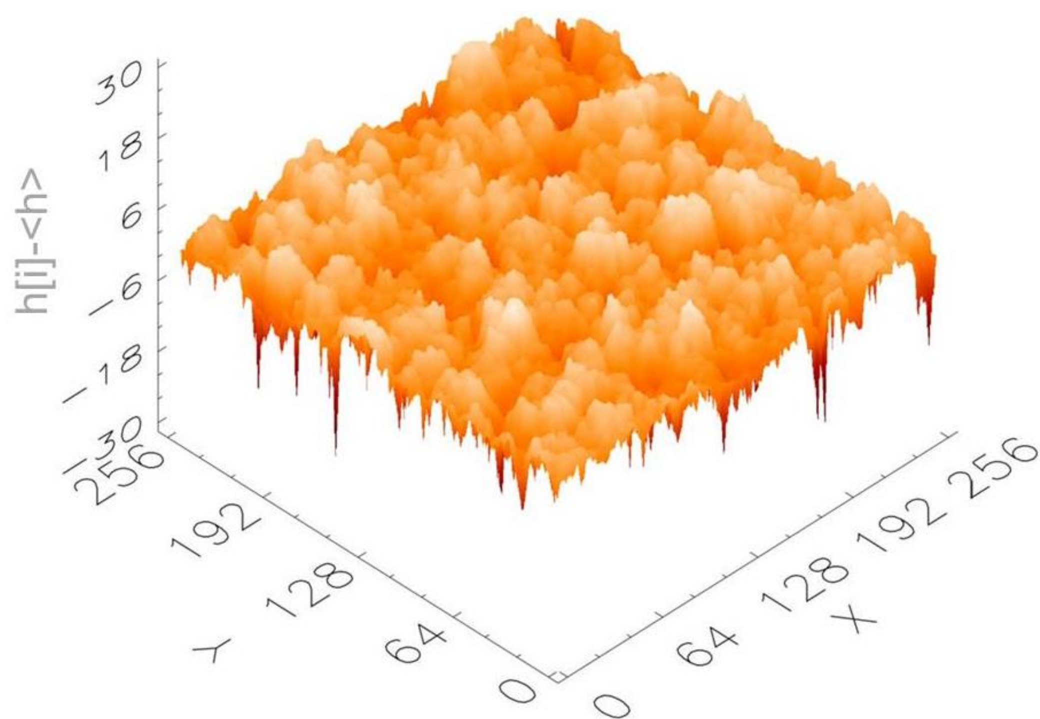

Figure 4.9: A typical film surface morphology of the film grown as in Fig. 4.8 then annealed at $T_A = 720\,\mathrm{K}$ with $E_d = 2.47\,\mathrm{eV}$ for the time $t_A = 10^4$ s.

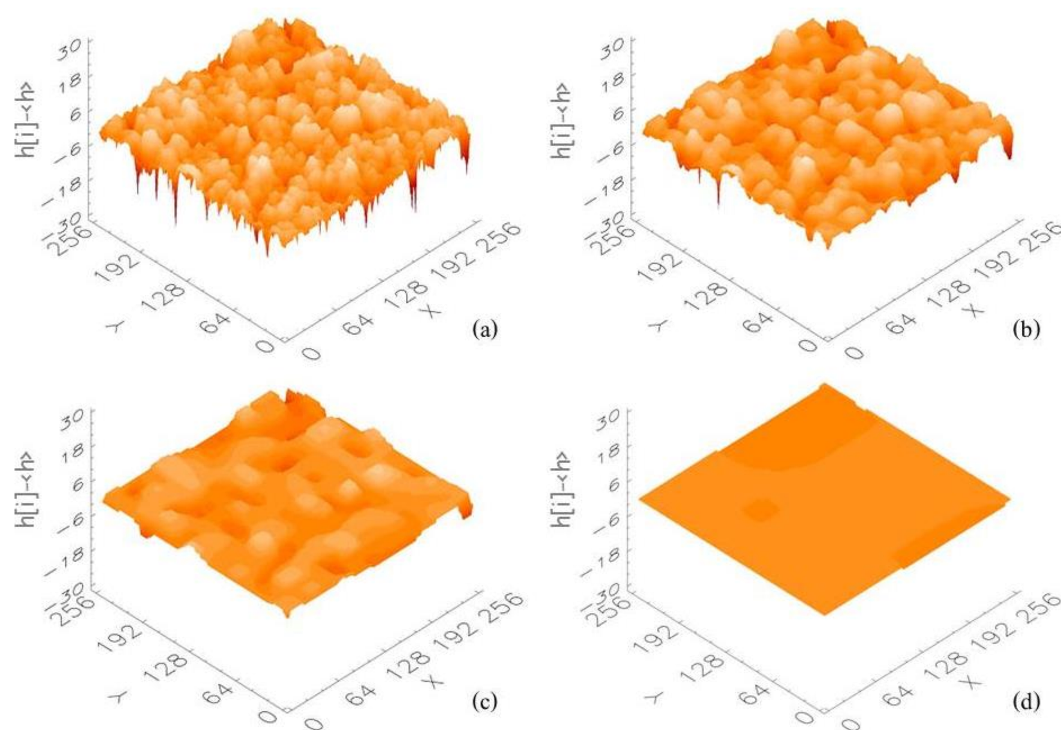

Figure 4.10: A typical film surface morphology of the film grown as in Fig. 4.8 then annealed with $E_d = 2.47\,\text{eV}$ for the time $t_A = 10^4\,\text{s}$ at (a) $T_A = 750\,\text{K}$ (b) $T_A = 800\,\text{K}$ (c) $T_A = 850\,\text{K}$ and (d) $T_A = 900\,\text{K}$.

To consider the global roughness of the film surfaces, the interface width W as a function of time t with and without desorption at various annealing temperatures are plotted and shown in Fig. 4.11. It can be seen that the W curves with desorption (opened symbols) go together with the curves without desorption (filled symbols). This indicates that the effect of desorption is much less than that of the annealing process, except at $T_A = 900\,\mathrm{K}$ where the W value of the film without desorption is smaller than the W value of the film with desorption at the end of the simulation. This implies that the surface of the film is rougher when the desorption process is included at this temperature, which is consistent with what is shown by the film surface morphologies.

To analyze the local roughness of the films annealed at $T_A = 900\,\mathrm{K}$ the height–height correlation functions as a function of the distance r for the cases with and without desorption are presented. The height difference correlations of the film with desorption (opened squares) clearly differs from the one without desorption (filled squares) as shown in Fig. 4.12. At this annealing temperature, the effect of the desorption process on the film becomes visible. The film surface with desorption is rougher than the one without desorption.

4.2.2 Effect of Desorption Energy

In the previous subsection, the desorption energy is kept fixed at $E_d = 2.47\,\mathrm{eV}$ while the annealing temperature is varied. In this subsection, effects of desorption energy is investigated by varying the value of E_d. Note that E_d should be larger than the activation energy, $E_0 + E_b$, required for a one–bonded atom to diffuse because it is obviously more difficult to remove a one–bonded atom completely out of the surface than to let it diffuses on the surface (Barabasi and Stanley, 1995). Since in this work $E_0 + E_b = 1.3\,\mathrm{eV}$, we choose to use 2 more values of E_d: $E_d = 2.3$ and $E_d = 2.4$ eV here. The larger E_d leads to larger desorption time τ, as shown in Table 4.2, which means smaller number of desorption. The annealing temperature is set at large enough values: $T_A = 850$ and $900\,\mathrm{K}$.

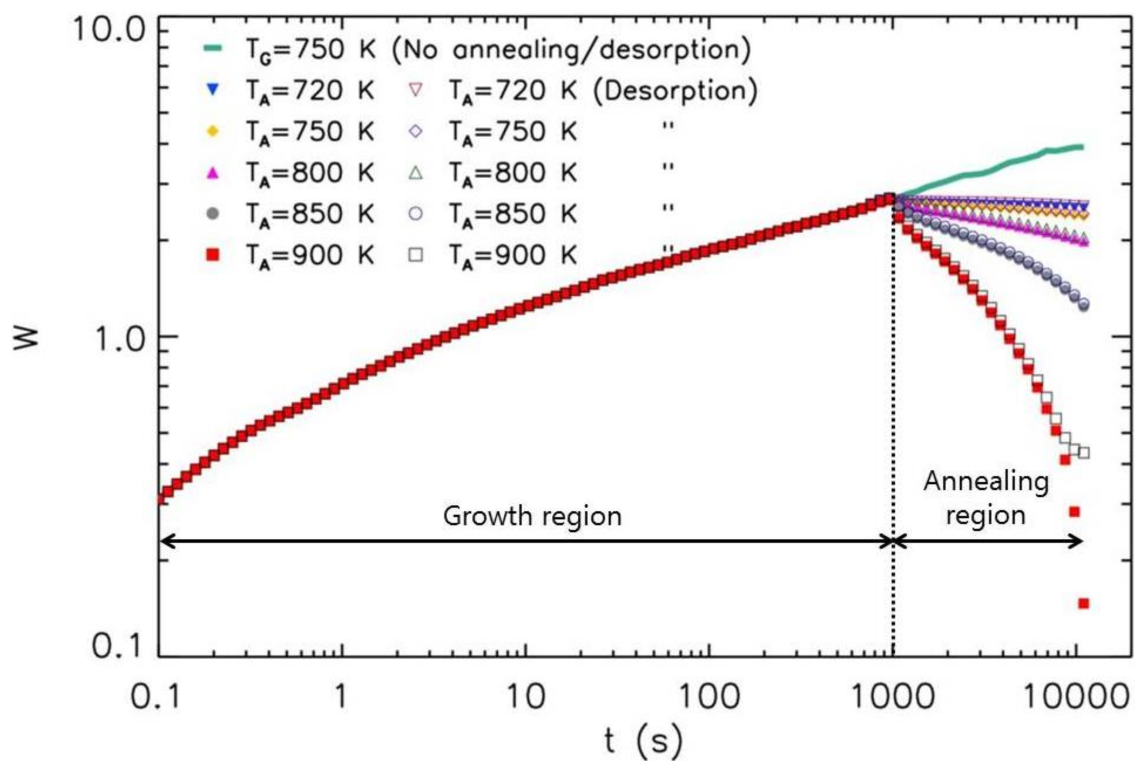

Figure 4.11: The interface width W versus time t of the MBE grown with $T_G = 750\,\mathrm{K}$ on a substrate 256×256 at the time $t_G = 10^3\,\mathrm{s}$ then annealed for the time $t_A = 10^4\,\mathrm{s}$ in using different T_A with (opened symbols) and without (filled symbols) desorption.

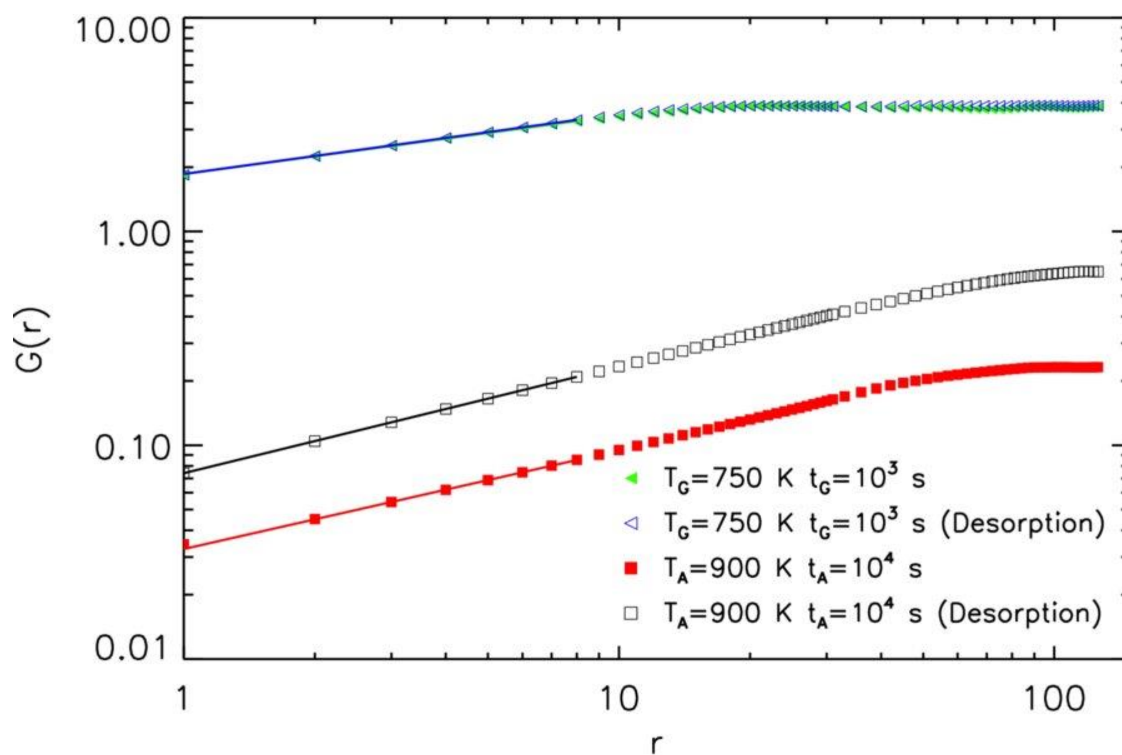

Figure 4.12: The height–height correlation function $G(r)$ as a function of separation r with (opened symbols) and without (filled symbols) desorption in the film grown at $T_G = 750\,\mathrm{K}$ then annealed at $T_A = 900\,\mathrm{K}$ for the time $t_A = 10^4$ s.

Table 4.2: Desorption time of atoms at various desorption energy when the substrate temperature is 850 K and 900 K.

T (K)	Desorption Time τ (s) with different E_d		
	2.30 eV	**2.40 eV**	**2.47 eV**
850	0.434	1.70	4.42
900	0.0758	0.275	0.678

The morphologies of films grown at $T_G = 750$ K for the time $t_G = 10^3$ s when the desorption energy E_d is chosen to be 2.3 and 2.4 eV are shown in Fig. 4.13. Their surfaces are not significantly different because only a small number of atoms are released from the grown film surfaces at $T_G = 750$ K (7 and 35 atoms when E_d is 2.4 and 2.3, respectively). This is confirmed by the average height of their surfaces, $\bar{h}$, being approximately equal to 1000 MLs, i.e. the average total number of deposited atoms on the surface. Although the desorption energy is varied in the film annealed for the time $t_A = 10^4$ s at $T_A = 850$ K, the film surfaces are still not different as shown in Fig. 4.14. In contrast, the surface of the film annealed at the highest annealing temperature $T_A = 900$ K for the time $t_A = 10^4$ s with the smaller E_d value (Fig. 4.15) is eroded. It is not significantly different from the one with a larger E_d (Fig. 4.10(d)), although our numerical calculation shows that 55.5% of atoms are removed from the interface at this high T_A.

The time evolution of the roughness of the film is displayed by the interface width W as a function time t in Fig. 4.16. The excellent agreement between the W curves of the films simulated with different E_d and annealed at $T_A = 850$ K (Fig. 4.16(a)) indicates a very small effect of the desorption energy on the film surface at this temperature. On the other hand, in the case of the film annealed at $T_A = 900$ K with various desorption energies, it can clearly be seen in the plot in Fig. 4.16(b) that the W values of the film at the time $t_A = 10^4$ s are different for each desorption energy. The interface width of the film with the smaller E_d is very large which indicates that its surface is very rough.

To consider the roughness at the time $t_A = 10^4$ s, the height difference correlation as a function of the separation distance r of the film annealed at $T_A = 900$ K is plotted. The local roughness, illustrated by $G-r$ plot in Fig. 4.17, is very different for each desorption energy. The value of G decreases when E_d is increased. This implies that the film annealed with $E_d = 2.4$ is rougher than the film annealed with larger E_d and the film annealed without desorption. We can conclude that the desorption energy has an effect on the film surface at high temperatures. However, its effect is much less significant than the effect of the annealing temperature.

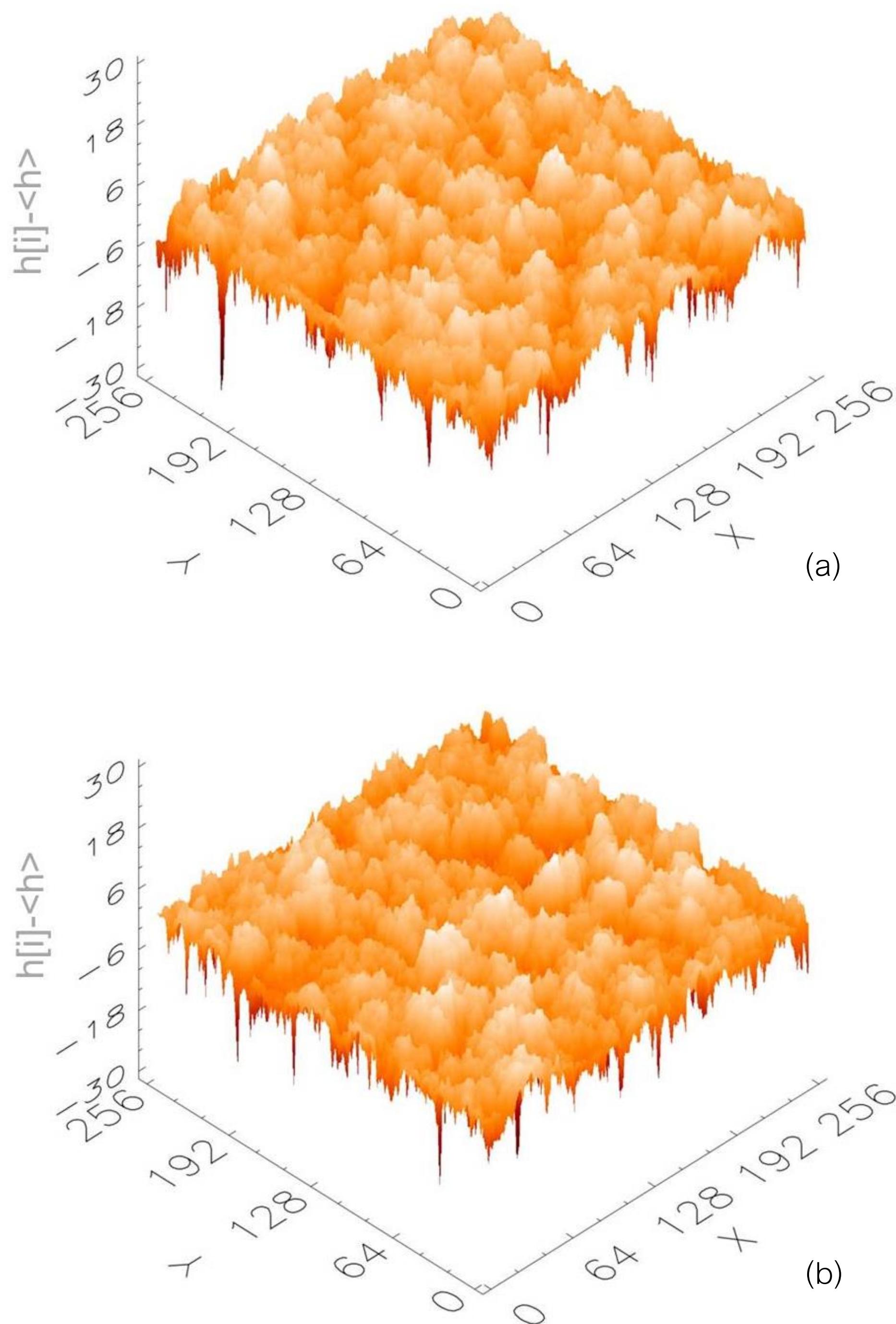

Figure 4.13: A typical morphology of MBE grown at $T_G = 750\,\text{K}$ when the desorption energy is (a) $E_d = 2.3\,\text{eV}$ and (b) $E_d = 2.4\,\text{eV}$ at the time $t_G = 10^3\,\text{s}$ in the system 256×256.

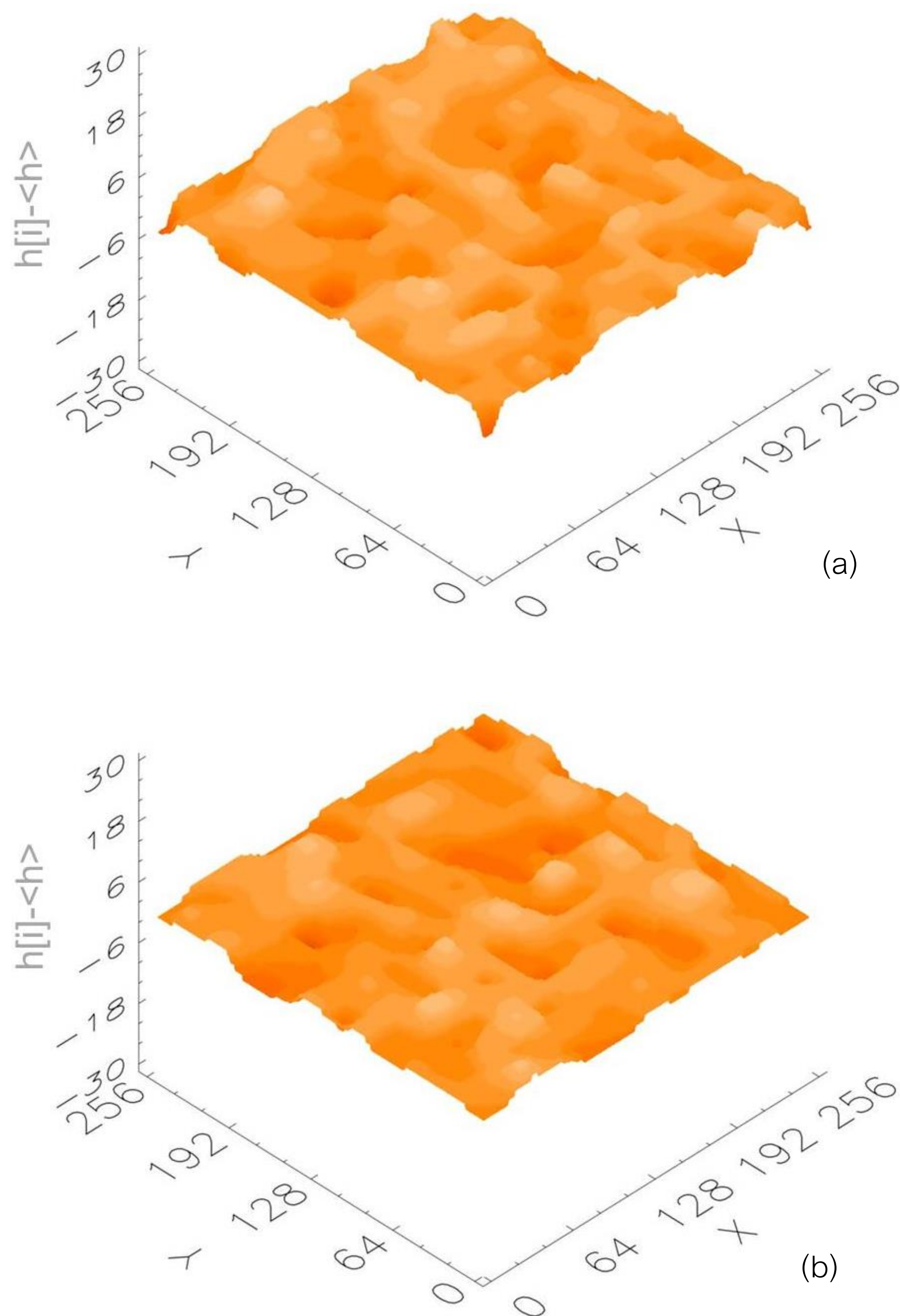

Figure 4.14: A typical morphology of the film in Fig. 4.13 then annealed at $T_A = 850\,\mathrm{K}$ for the time $t_A = 10^4$ s when the desorption energy is (a) $E_d = 2.3\,\mathrm{eV}$ and (b) $E_d = 2.4\,\mathrm{eV}$.

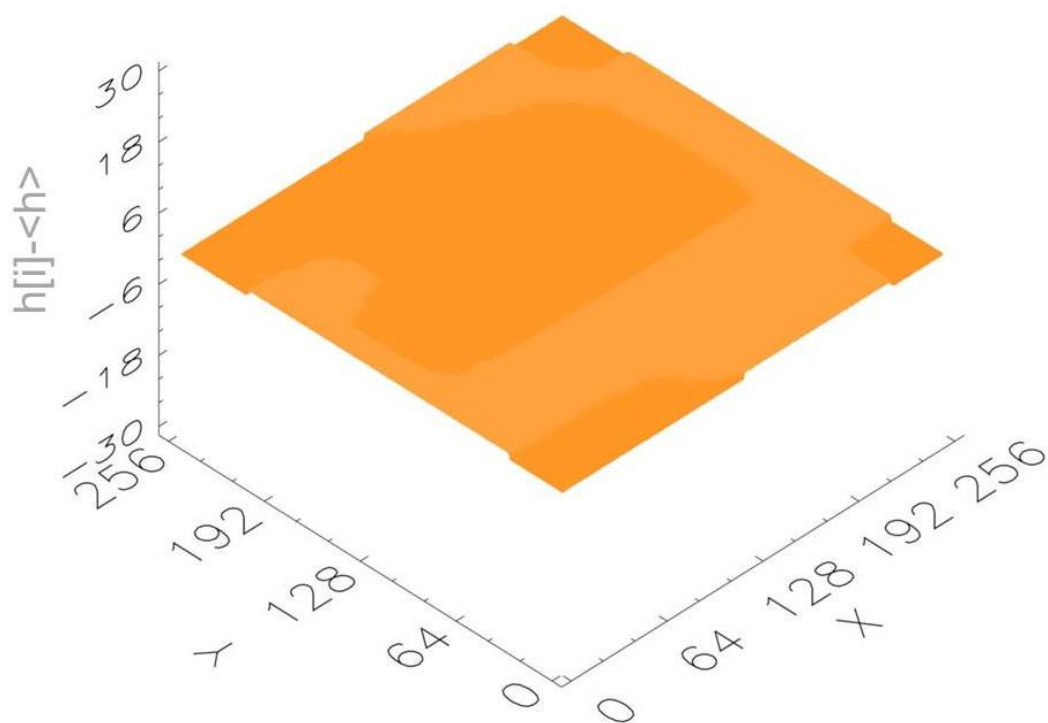

Figure 4.15: A typical morphology of the film in Fig. 4.13(b) then annealed at $T_A = 900$ K for the time $t_A = 10^4$ s when the desorption energy is $E_d = 2.4$ eV.

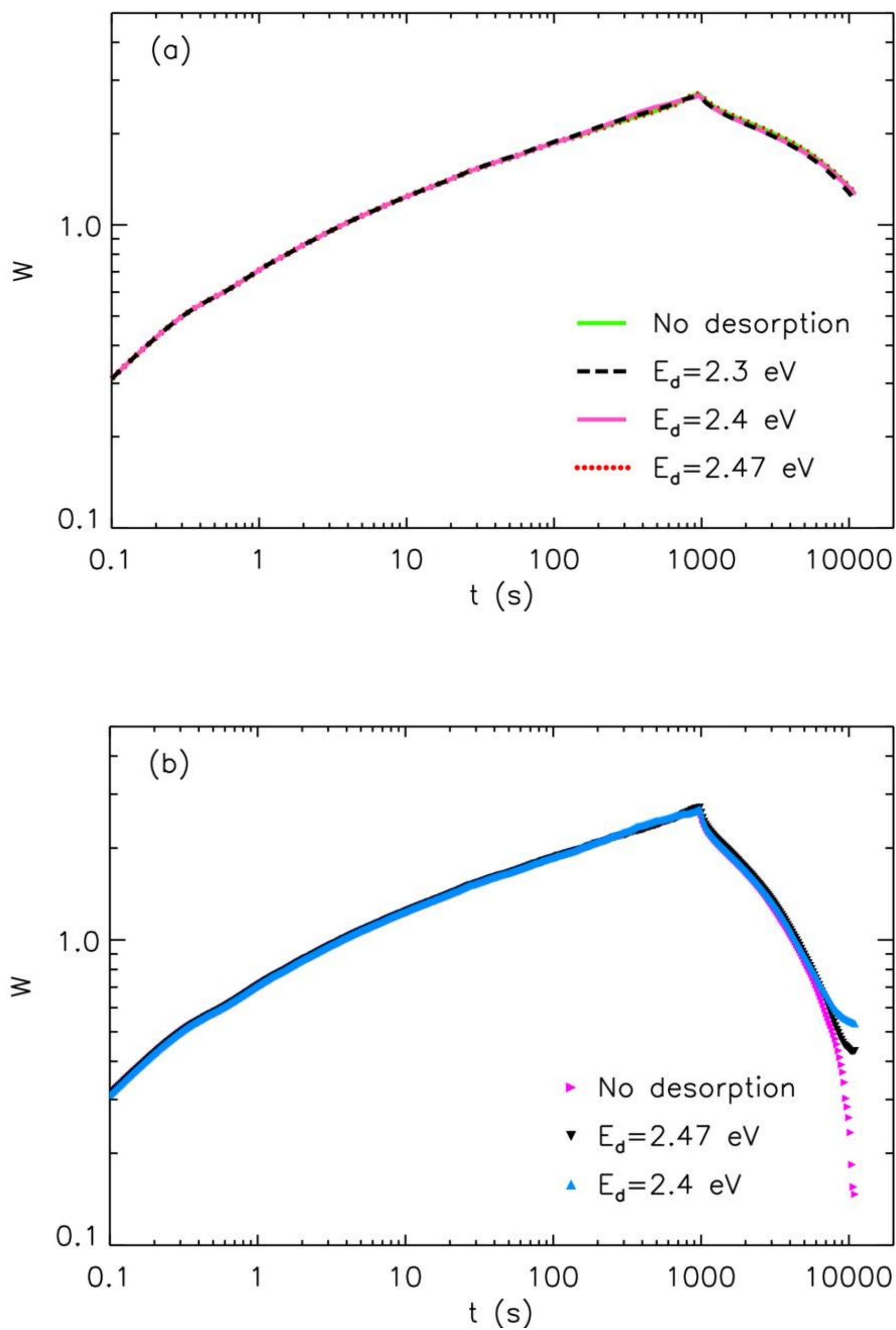

Figure 4.16: The interface width $W(t)$ as a function of time in the MBE growth with $T_G = 750\,\mathrm{K}$ at the time $t_G = 10^3\,\mathrm{s}$ then annealed for the time $t_A = 10^4\,\mathrm{s}$ with a) $T_A = 850\,\mathrm{K}$ and b) $T_A = 900\,\mathrm{K}$ when the desorption energy is varied.

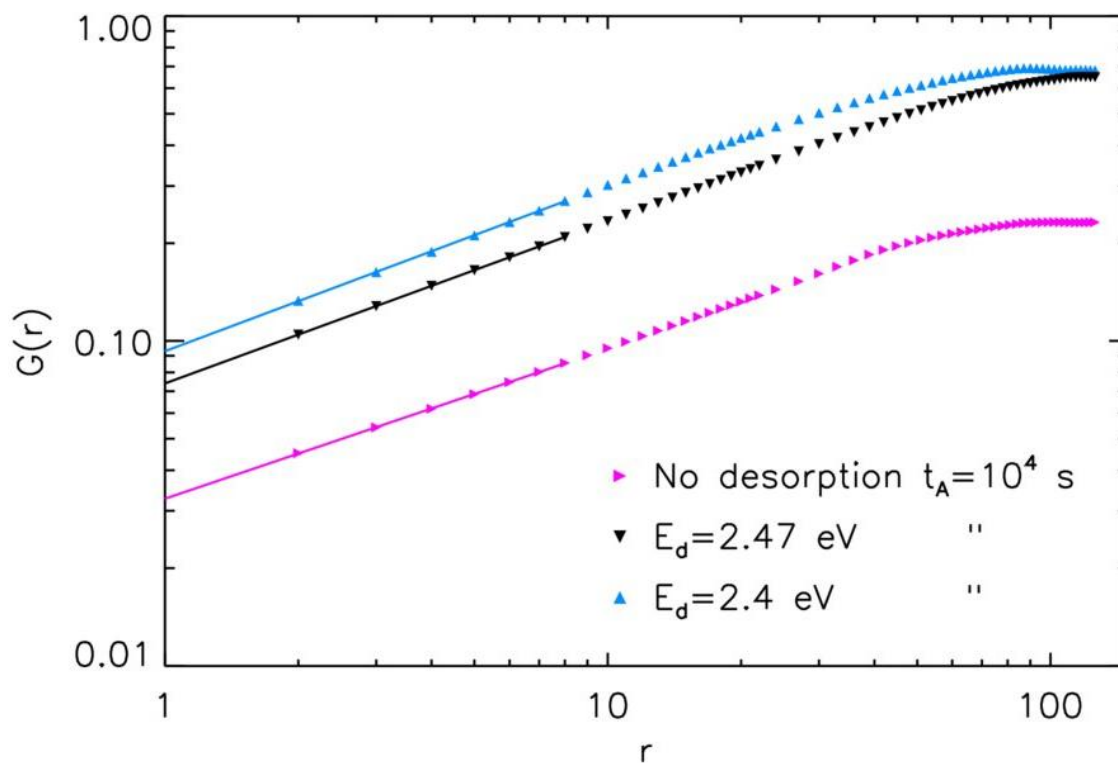

Figure 4.17: The height–height correlation function $G(r)$ as a function of separation r for MBE growth on a substrate 256×256 with $T_G = 750$K at the time $t_G = 10^3$ s then annealed for the time $t_A = 10^4$ s with $T_A = 900$ K when the desorption energy is $E_d = 2.4$ and 2.47 eV.

CHAPTER V

CONCLUSIONS

The main purpose of this work is to study effects of the annealing process on a film surface grown by MBE model when the diffusion of surface atoms is modeled by Arrhenius law. In the first case, desorption of atoms is assumed to be negligible. Roughness of the film surfaces is investigated via the film surface morphology, the time evolution of the interface width, and the height–height correlation functions. Our simulation results show that the morphologies become smoother and the values of interface width and height–height correlation functions become smaller when higher annealing temperatures are used. These lead to a conclusion that the film surface is smoother as the annealing temperature is increased, and the film surface is smoothest at $T_A = 900$ K, i.e. the highest temperature considered. This is because thermal energy from the substrate is sufficient for atoms to break bonds formed during deposition process and diffuse to other positions. According to the Arrhenius hopping rate in chapter 2, the diffusion of atoms increases when the temperature is increased. This signifies that the chance of an atom to diffuse to position with large coordinate numbers is the greatest at the highest annealing temperature. Moreover, we conclude that the film grown by MBE model exhibits multi-affine scaling behavior from evidence of q–dependent roughness exponents in the generalized q^{th} correlation function $G_q(r)$ plot. Although the annealed film is very smooth, it still demonstrates the strong multifractality in the same way as the rough as–grown films.

We also consider effects of the desorption process on the film surface by analyzing of the statistical properties as in the first case. The global roughness, illustrated in the plot of the interface width W as a function time t, indicates that the effect of desorption is extremely small. This is because the W curves with desorption overlap very well with the W curves of the system without desorption. Even when the desorption energy is decreased in order to promote a large number of atomic desorption from the interface, the global roughness of the films is still indifferent at a moderate temperature. At $T_A = 900$ K, however, the film is affected by the

desorption process as can be observed in the film surface morphologies. The surface of film annealed with desorption is deteriorated since large number of atoms are removed from the surface. When we consider the local roughness of the film surface with and without desorption at $T_A = 900$ K from the height–height correlation function $G(r)$ plot, the effect of the desorption process on the film can be obviously seen. The film surface with desorption is much rougher than the one without desorption. In addition to annealing at $T_A = 900$ K, the lower desorption energy E_d causes the surface to be very rough due to the fact that the smaller E_d leads to a smaller desorption time τ , which means more occurrence of desorption.

Finally, we note the possibility of choosing different values of the activation energy E_d for atoms to be removed from the interface. This subject leads to an interesting question of how many desorption energy values can be used without deforming the film surface. Our future research direction is to extend the annealing time duration and to experiment with the value of desorption energy which is lower than the value used in this dissertation in order to study effects of the low desorption energy on the film surface. Moreover, we also plan to decrease the annealing temperature and increase the annealing time instead.

REFERENCES

Aarão Reis, F. D. A. (2010). Dynamic scaling in thin–film growth with irreversible step–edge attachment. *Phys. Rev. E* 81: 041605.

Arthur, J. R. (2002). Molecular Beam Epitaxy. *Surf. Sci.* 500: 189.

Barabási, A. L., Bourbonnais, R., Jensen, M., Kertész, J., Vicsek, T., and Zhang, Y. –C. (1992). Multifractality of growing surfaces. *Phys. Rev. A* 45: R6951.

Barabási, A. L., and Stanley, H. E. (1995). *Fractal concepts in surface growth*. New York: Cambridge University Press.

Barabási, A. L., Szépfalusy, P., and Vicsek, T. (1991). Multifractal spectra of muti–affine functions. *Physica. A* 178: 17.

Barabási, A. L., and Vicsek, T. (1991). Multifractality of self-affine fractals. *Phys. Rev. A* 44: 2730.

Chaiyasorn, C. (2007). *Ballistic deposition model with surface diffusion for thin film growth on patterned substrates*, Master's thesis, Master's thesis, Department of Physics, Faculty of Science, Chulalongkorn University.

Chanyawadee, S. (2004). *Modeling of molecular beam epitaxy growth under Ehrlich–Schwoebel potential barrier effects*, Master's thesis, Department of Physics, Faculty of Science, Chulalongkorn University.

Changkaew, P. (2009). *Thin film growth simulation with reduction techniques in (2+1) dimensional substrate systems*. Master's thesis, Department of Physics, Faculty of Science, Chulalongkorn University.

Chatraphorn, P. P. (2000). *Understanding kinetic surface roughening using local, discrete, nonequilibrium, growth models*. Doctoral Dissertation, Department of Physics, Faculty of Science, University of Maryland.

Dasgupta, C., Das Sarma, S., and Kim, J. M. (1996). Controlled instability and multiscaling in models of epitaxial growth. *Phys. Rev. E* 54: R4552.

Das Sarma, S., Ghaisas, S. V., and Kim, J. M. (1994). Kinetic super–roughening and anomalous dynamic scaling in nonequilibrium growth models. *Phys. Rev. E* 49: 122.

Das Sarma, S., Lanczycki, C. J., Ghaisas, S. V., and Kim, J. M. (1994). Defect formation and crossover behavior in the dynamic scaling properties of molecular–beam–epitaxy. *Phys. Rev. B* 49: 10693.

Das Sarma, S., Lanczycki, C. J., Kotlyar, R., and Ghaisas, S. V. (1996). Scale invariance and dynamical correlations in growth models of molecular beam epitaxy. *Phys. Rev. E* 53: 359.

Das Sarma, S., and Tamborenea, P. (1991). A new universality class for kinetic growth: One–dimensional molecular–beam epitaxy, *Phys. Rev. Lett.* 66: 325.

Elsholz, F., Meixner, M., and Schöll, E. (2003). Kinetic Monte Carlo Simulation of Self Organized Pattern Formation in Thin Film Deposition. *Nucl. Instr. and Meth. in Phys. Res. B.* 202: 249.

Family, F., and Vicsek, T. (1985). Scaling of the active zone in the Eden process on percolation networks and the ballistic deposition model. *J. Phys. A* 18: L75.

Ghaisas, S. V., and Das Sarma, S. (1992). Surface Diffusion Length under Kinetic Growth Conditions. *Phys. Rev. B* 46: 7308.

Hong, W. –K., et al. (2008). Effects of surface roughness on the electrical characteristics of ZnO nanowire field effect transistors. *Appl. Surf. Sci.* 254: 7559.

Johari, G. P., (1982). Effect of annealing on the secondary relaxations in glasses. *J. Chem. Phys.* 77: 4619.

Kim, S. –P., Lee, K. –R., Chung, Y. –C., Sahashi, M., and Kim, Y. K. (2009). Molecular dynamics simulation study of deposition and annealing behaviors of Al atoms on Cu surface. *J. Appl. Phys.* 105: 114312.

Kittel, C. (1971). *Introduction to Solid State Physics*. New York: John Wiley & Sons Inc.

Krug, J. (1994). Turbulent interfaces. *Phys. Rev. Lett*. 72: 2907.

López, J. M. (1999). Scaling approach to calculate critical exponents in anomalous surface roughening. *Phys. Rev. Lett*. 83: 4594.

Ohring, M. (2002). *Materials science of thin films: Deposition and Structure*. Ed. 2nd, San Diego: Academic Press.

McCulloch, D. G., and Merchant, A. R. (1996). The effect of annealing on the structure of cathodic arc deposited amorphous carbon nitride films. *Thin Solid Films* 290–291: 99.

Meng, B., and Weinberg, W. H. (1996). Dynamical Monte Carlo studies of molecular beam epitaxial growth models: interfacial scaling and morphology. *Surf. Sci.* 364: 151.

Neave, J. H., Dobson, P. J., Joyce, B. A., and Zhang, J. (1985). Reflection high–energy electron diffraction oscillations from vicinal surfaces–a new approach to surface diffusion measurements. *Appl. Phys. Lett.* 47: 100.

Palisaitis, J., and Vasiliauskas, R. (2008). *Growth of thin films*. Sweden: linköping University.

Pimpinelli, A., and Villain, J. (1998). *Physics of Crystral Growth.* New York: Cambridge University Press.

Schinzer, S., Köhler, S., and Reents, G. (2000). Ehrlich–Schwoebel barrier controlled slope selection in epitaxial growth. *Eur. Phys. J. B* 15: 161.

Tan, E. P. S., and Lim, C. T. (2006). Effects of annealing on the structural and mechanical properties of electrospun polymeric nanofibres. *Nanotechnology* 17: 2649.

Tanaka, M., Suzuki, T., and Nishinaga, T. (1991). Surface diffusion of Al and Ga atoms on GaAs (001) and (111)B vicinal surface in molecular beam epitaxy. *J. Cryst. Growth* 111: 168.

Xiao, R. –F., Alexander, J. I. D., and Rosenberger, F. (1991). Growth morphologies of crystal surfaces. *Phys. Rev. A* 43: 2977.

Xiao, R. –F., and Ming, N. –B. (1994). Surface roughening and surface diffusion in kinetic thin–film deposition. *Phys. Rev. E* 49: 4720.

VITAE

Miss Somjintana Potepanit was born on November 6, 1987 in Mae Hong Son, Thailand. She graduated from Chulalongkorn University with a bachelor's degree of science in Physics on March 16, 2010. She has continued to study a Master's degree at Chulalongkorn University in 2010.

CONFERENCE PRESENTATIONS

- Siam Physics Congress SPC2012 — Phra nakhon Si Ayutthaya, Thailand

  Poster Presentation — May 9 – 12, 2012

  - Effects of Annealing on Thin Film Grown by Molecular Beam Epitaxy Modeled with Arrhenius Law : S. Potepanit and P. Chatraphorn

- Graduate Research Conference GRC2013 — Khon Kaen, Thailand

  Oral Presentation — February 21, 2013

  - Correlation Functions in Annealed Film Surface Grown by Molecular Beam Epitaxy Model : S. Potepanit and P. Chatraphorn

- Siam Physics Congress SPC2013 — Chiang Mai, Thailand

  Poster Presentation — March 21 – 23, 2013

  - Effects of Annealing Process with and without Desorption Process on Film Surfaces Grown by MBE Model with Arrhenius Law : S. Potepanit and P. Chatraphorn

PUBLICATION

- Thai Physics Society (Thai J. Phys.) — Thailand

  Thai Journal of Physics, Series 8 — May 9 – 12, 2012

  - Effects of Annealing on Thin Film Grown by Molecular Beam Epitaxy Modeled with Arrhenius Law : S. Potepanit and P. Chatraphorn

PROCEEDING PUBLICATION

- Graduate Research Conference GRC2013 — Khon Kaen, Thailand

  Khon Kaen University — February 21, 2013

  - Correlation Functions in Annealed Film Surface Grown by Molecular Beam Epitaxy Model : S. Potepanit and P. Chatraphorn